

COMPUTER FINITE ELEMENT SIMULATION  
IN MECHANICAL DESIGN

By

Ryan Christopher Russell

Thesis

Submitted to the Faculty of the  
Graduate School of Vanderbilt University  
in partial fulfillment of the requirements  
for the degree of

MASTER OF SCIENCE

in

Mechanical Engineering

December 2013

Nashville, Tennessee

Approved:

Thomas J. Withrow, Ph.D.

Haoxiang Luo, Ph.D.

Michael Goldfarb, Ph.D.

To my friends and family, who have supported me through every step of my journey  
and  
To Meredith, who has been patient and loving throughout

# TABLE OF CONTENTS

	Page
DEDICATION.....	ii
LIST OF TABLES.....	v
LIST OF FIGURES.....	vi
Chapter	
I. Introduction .....	1
1. A History of Finite Element Analysis.....	1
2. What is FEA?.....	5
3. FEA Validation, Takeaways, and Use in the Design Cycle .....	7
II. Modeling and Analysis for the Adaptive Vehicle Make.....	10
1. AVM Background.....	10
2. Main Chassis.....	16
2.1 Static Structural Study .....	18
2.2 Modal Vibration Study.....	24
2.3 Thermal Study .....	26
3. Front Bumper.....	29
3.1 Impact Study.....	31
3.2 Modal Vibration Study.....	39
4. Conclusions.....	40
III. Modeling and Analysis of Brushless DC Motor Failure .....	43
1. System Redesign and Motor Background .....	43
2. Modeling the Motor.....	47
3. FEA Study.....	50
3.1 Inputs .....	51
3.2 Results .....	57
4. Validating the Model .....	62
5. Redesign Solution and Optimization .....	68
6. Optimized Prototype .....	80

7. Conclusions.....	88
IV. Conclusions and Future Works.....	92
Appendix	
A: Chassis Modal Shapes.....	95
B: Bumper Modal Shapes .....	96
C: Maxon EC Flat Motor Data Sheet.....	97
D: Maxon EC Flat Motor Pin Schematic .....	98
E: Gap Pad 1500 Data Sheet.....	99
References.....	100

## LIST OF TABLES

TABLE	PAGE
1: MOTOR COMPONENT THERMAL PROPERTIES .....	53
2: HEAT GENERATION FOR DIFFERENT LOADING CONDITIONS .....	55
3: MAXIMUM COIL TEMPERATURE AT VARIOUS LOADS .....	60
4: AVERAGED 1 AMP COIL TEMPERATURE OVER TIME (34.4 °C STEADY STATE).....	64
5: AVERAGED 2 AMP COIL TEMPERATURE OVER TIME (68.1 °C STEADY STATE).....	65
6: AVERAGED 3 AMP COIL TEMPERATURE OVER TIME (133.8 °C STEADY STATE).....	65
7: COMPARING ANSYS AND EXPERIMENTAL RESULTS .....	66
8: GAP PAD WIDTH AND DIAMETER DESIGN POINTS WITH RESULTING COIL TEMPERATURE .....	73
9: MOTOR WITH ALUMINUM CONTACTS MAXIMUM COIL TEMPERATURE AT VARIOUS LOADS .....	77
10: MOTOR WITH GAP PAD AND ALUMINUM CONTACTS MAXIMUM COIL TEMPERATURE .....	79
11: COMPARISON OF MAXIMUM COIL TEMPERATURES (°C) .....	87
12: COMPARING ANSYS AND EXPERIMENTAL RESULTS FOR EACH PROTOTYPE .....	90

## LIST OF FIGURES

Figure	Page
1: VEHICLE WITH CHASSIS AND BUMPER LOCATIONS LABELED .....	16
2: MAIN CHASSIS CAD GEOMETRY .....	17
3: CHASSIS LOADS AND SUPPORTS .....	20
4: CHASSIS STRESS (MPA) .....	22
5: CHASSIS DEFORMATION (METERS) .....	23
6: CHASSIS TEMPERATURE PROFILE (°C) .....	28
7: FRONT BUMPER CAD GEOMETRY .....	30
8: FENDER BENDER BUMPER DEFORMATION (MM) .....	34
9: LOW SPEED CASE BUMPER FACTOR OF SAFETY .....	34
10: WORST CASE SCENARIO BUMPER DEFORMATION (MM) .....	35
11: WORST CASE SCENARIO FACTOR OF SAFETY .....	36
12: SURFACE AREA OF FORCE APPLIED TO BUMPER .....	36
13: FRONT BUMPER WITH POINT LOAD .....	37
14: BUMPER FACTOR OF SAFETY RESULTS UPDATED FOR IMPACT POINT .....	38
15: SPEED VERSUS TORQUE CURVE FOR MAXON EC 244879 .....	46
16: MAXON EC 244879 .....	47
17: CAD MOTOR AND ACTUAL MOTOR WITHOUT COVER .....	49
18: VIEWS OF ACTUAL MOTOR AND CAD MOTOR WITH AND WITHOUT COVER .....	49
19: TEMPERATURE PROFILE OF MOTOR (1 AMP CONDITION) .....	58
21: COIL FAILURE ON OLD MOTOR DUE TO OVERHEATING .....	61
22: EXPERIMENTAL SETUP .....	63
23: COIL TEMPERATURE AS A FUNCTION OF TIME FOR VARIOUS APPLIED CURRENTS .....	66
24: IMAGE SHOWING MINOR COIL FAILURE FROM 3 AMP LOAD .....	68
25: INNER BASE TOTAL HEAT FLUX .....	69
26: CIRCUIT BOARD TOTAL HEAT FLUX .....	71
27: TOP VIEW OF MOTOR WITH GAP PAD INSERT .....	72
28: MAXIMUM TEMPERATURE AS A FUNCTION OF WIDTH AND DIAMETER OF GAP PAD (VIEW 1) .....	74
29: MAXIMUM TEMPERATURE AS A FUNCTION OF WIDTH AND DIAMETER OF GAP PAD (VIEW 2) .....	75
30: CAD MODEL OF MOTOR WITH ALUMINUM CONTACTS .....	76
31: CAD MODEL OF MOTOR WITH GAP PAD AND ALUMINUM CONTACTS .....	78
32: MOTOR CIRCUIT BOARD .....	81
33: MOTOR CIRCUIT BOARD WITH GAP PAD INSERT .....	82
34: MOTOR WITH GAP PAD AND REROUTED WIRING .....	83
35: MOTOR WITH ALUMINUM CONTACTS .....	84
36: MOTOR WITH GAP PAD AND ALUMINUM CONTACTS .....	85

37: 1 AMP MAXIMUM COIL TEMPERATURE COMPARISON .....	86
38: 2 AMP MAXIMUM COIL TEMPERATURE COMPARISON .....	86
39: 3 AMP MAXIMUM COIL TEMPERATURE COMPARISON .....	87

## CHAPTER I

### **Introduction**

#### 1. A History of Finite Element Analysis

“The central activity of engineering, as distinguished from science, is the design of new devices, processes and systems” [Tribus]. Design has always been, and will continue to be, one of the most important facets of the field of engineering.

The finite element method, one tool used for design, is a numerical method that is applied to real world problems involving complicated phenomenon to solve engineering problems [Reddy 2006], [Logan]. An examination of the finite element process first requires a look back at the history of the method to see how we got to modern day finite element analysis. A fundamental historical perspective can also help increase the users understanding of the finite element tool.

The method of representing a domain as a collection of discrete parts can be traced back as far as ancient mathematicians in their estimations of the value of  $\pi$  to the accuracy of nearly 40 significant figures by representing a circle as a polygon of a very large but finite number of sides [Reddy 1978]. In 1851, Schellback discretized a surface into finite right triangles and wrote a finite difference expression to solve for the total area in an attempt to determine the surface of minimum area bound by a closed curve in space [Williamson]. Later, in 1906, researchers in Germany discovered that a body having several bars in a regular pattern behaves like an isotropic elastic body



[Wieghardt], [Riedel]. These examples show early applications in which bodies were discretized into “finite elements” to solve problems.

The modern development of the finite element method began in 1940s in the field of aircraft structural engineering. Aircraft fuselages and wings were treated as assemblies of strings, skins, and shear panels, which were represented by a framework of one dimensional bars and beams to solve for stresses and bending over the continuous solid. This work, done by Hrennikoff in 1941 [Hrennikoff] and McHenry in 1943 [McHenry], was known as the framework method. The framework method is largely regarded as a precursor to FEA as it works well for framed structures but cannot be applied to oddly shaped members, nor does it discretize a body into smaller pieces but rather substitutes members of a different type [Cook].

The modern finite element method can be further traced through the works of Courant, who determined the torsional rigidity of a hollow shaft by dividing the cross section using piecewise shape functions into triangular subunits and then solving a stress function over each triangle at certain net-points, or nodes as they are now known [Courant]. In 1947, Levy developed the flexibility method [Levy 1947], and published a work in 1953 suggesting the stiffness method as an alternative for use in statically redundant aircraft structures [Levy 1953]. His stiffness method, although successful, was too bulky to solve by hand, and did not become popular until the development of the high speed computer.

Engineers debate as to which of the works of Hrennikoff, Courant, or even Levy represent early forms, or rather precursors to the finite element method, but each of their works have certain key features of the modern day method. The formal presentation of

the method came about later in the 1950s and early 1960s, starting with Turner, Robinson, and Argyris, who each worked with two dimensional elements, including three-node triangular elements, and used these elements to derive stiffness matrices for the procedure now known as the direct stiffness method [Turner 1956], [Robinson], [Argyris 1960].

The phrase “finite element” was not used until 1960 when Clough used both three and four node elements to solve plane stress analysis problems [Clough 1960]. In the years thereafter, many new techniques and elements were developed. In 1961, Melosh developed a flat, rectangular-plate bending-element stiffness matrix [Melosh 1961]. A similar curved-shell version for axisymmetric shells and pressure vessels was developed in 1963 by Grafton and Strome [Grafton].

The finite element method was extended to three-dimensional problems by using tetrahedral elements in the early 1960s [Martin 1961], [Gallagher 1962], [Melosh 1963]. Later, additional three dimensional elements were used [Argyris 1964] and methods for axisymmetric solids were developed in 1965 [Clough 1965], [Wilson 1965].

It must be noted that all of the aforementioned works dealt with small scale strains and displacements, elastic behavior, and static conditions. However, works on large deflection and thermal analysis [Turner 1960], nonlinear materials [Gallagher 1962], buckling [Gallagher 1963], distributed-mass systems [Archer], and visco-elasticity [Zienkiewicz 1965] were also performed in the 1960s.

Another big development in the finite element method was the use of variational formulation to set up problems to allow for the solving of non-structural applications and field problems [Melosh 1963]. This allowed for the use of the finite element method to

solve fluid flow, heat conduction, and torsion problems for shafts [Zienkiewicz 1968], [Martin 1968], and [Wilson 1966]. The method was further expanded when Szabo and Lee developed the weighted residual method in 1969 [Szabo] and Zienkiewicz and Parekh used it to solve transient field problems in 1970 [Zienkiewicz 1970].

These works in the 1960s outlined the basis for many of the methods and techniques that are core to the modern finite element method. However, many of the applications of these methods were limited by computing power, as equations with tens of thousands of degrees of freedom are not solvable by hand. Therefore, the development of finite element methods is linked closely with the development of computing power [Hughes]. General finite element computer programs began appearing in the late 1960s and early 1970s. In the late 1970s, computer graphics had advanced enough to advent the use of finite element software for actual design, rather than simply completed design verification or structural failure analysis [Cook]. More about the use of computer FEA software in the design cycle will be discussed later.

With modern advances in finite element software, graphics, and computing power, it is sometimes easy to forget what is behind these powerful software programs. A look back at the history and fundamentals of the finite element method can greatly help an engineer understand the logic behind the tool, which greatly increases its power, accuracy, and reliability. This fundamental understanding of the finite element method and how it makes the tool more effective will be evident in the following studies.

## 2. What is FEA?

The acronym FEA stands for finite element analysis. At its basis, FEA is a numerical method used to solve engineering field problems by dividing a domain into several smaller *finite* subdomains, which each act as individual *elements* over which algebraic equations are applied and an approximate solution is given using the finite difference method. The results from each finite element are then reassembled and different types of *analysis* can be run to solve any number of complicated engineering problems using this method and a powerful solver [Reddy 2006].

The basic method by which a problem is solved using FEA can be broken down into several steps [Cook]. First, the problem must be identified and classified. There are several different types of analysis that can be performed. Selecting the correct analysis for the correct problem is important. Next, a simplified mathematical model should be derived from which to build the basic physical concepts of the analysis. Preliminary analysis is then performed, in which a solution is obtained to help ballpark the result sought after from the FEA study. The next step is to actually perform the finite element analysis, which is almost always done with the aid of a computer. The final step is to check the results. It is important to first note if the results “look” correct, if they make sense, and if they are similar to the preliminary analysis performed. It may also be necessary to check the results against other solution forms, or against a physical model [Cook]. It must also be noted that the FEA process is a very iterative one. Rarely is the first FEA study the final one, and revisions are often needed after interpreting the results of a study.

The actual FEA portion of the solution method described above can be broken down into eight steps, many of which are typically performed by a computer. The first step is to break the system into “finite elements” by discretizing the system into several elements formed by associated nodes. There are a variety of different types and shapes of elements available for use, depending on the geometry of the system. The second step is to select a displacement function to fit each element. The strain-displacement and stress-strain relationships are then selected in the third step, which is dependent on the material properties of each element. Fourth, the stiffness matrix equations are derived by the computer, and fifth, they are assembled into a global matrix with all elements and boundary conditions incorporated. Sixth, the equations are solved simultaneously to determine the displacement at each node. Consequently, the seventh step is to then calculate the stress and strain for each element using the relationships determined before the equation assembly. Finally, the eighth step is to interpret the results, a vague but important task that will be discussed in more detail later [Logan]. This method is a general one, and there are multiple ways that it is implemented in different FEA computer programs.

On a larger scale, the method can be broken down into preprocessing, numerical analysis, and post-processing [Cook]. Preprocessing refers to all the data input by the user related to the geometry, material properties, element types and mesh, loads, supports, boundary conditions, etc. The numerical solution step is then performed by a computer. This step was broken down into parts above, and consists of the processor combining the equations into matrix form and then solving simultaneously. Finally, post-

processing occurs, in which the results are displayed in graphical form. The information is automatically generated once requested by the user.

The use of FEA provides several advantages over other solution and modeling methods. First, by dividing a system into small parts, systems with complex geometries or several materials can be easily represented in one model. This provides a huge advantage over traditional analysis methods and allows engineers to solve unique problems which would have required much simplification years ago. The size of the elements can also be varied throughout the model to increase or decrease resolution in areas that need to be more closely examined or are not important to the result. Additionally, the method can handle general load conditions and an unlimited number and types of boundary conditions. The method can also handle a large variety of problems, including heat transfer, stress analysis, dynamic problems, and nonlinear problems.

### 3. FEA Validation, Takeaways, and Use in the Design Cycle

The finite element method has been discussed in detail, both its origin and its basic operation. However, any numerical simulation, such as FEA, is not an end in itself, but rather an aid in the design and manufacturing process. Therefore, it is important to understand not only the tool but how it can be used effectively to solve engineering problems [Reddy 2006].

As mentioned, the FEA tool was not used in design until the late 1970s, when computer graphics were attached to FE software [Cook]. The enhanced graphics allowed the user to quickly view the results of a study, and then manipulate the original system.

This process creates an iterative cycle of analysis, drawing conclusions, redesigning the system, and then reanalyzing. This iterative process is a common one in the design world. Using FEA tools rather than experimentation or rough hand calculations shortens the design process. The earlier in the design process that finite element tools can be used, the quicker, cheaper, safer, and more efficient the design will be.

Clearly, the finite element method is a powerful tool capable of solving complicated problems quickly and with graphically impressive results. However, this ease of use leads to one of its biggest weaknesses, an overly trusting attitude towards the results of an FEA study.

Finite element analysis users sometimes have naïve faith in computer programs and value computer skills over traditional “ballparking” analytical methods [Cook]. This brings up the importance of learning how to use FEA as a tool rather than blindly accepting its results as fact.

A study of computer misuse in engineering showed that of 52 cases in which incorrect analysis results caused damage, 58 percent were due to user error [Computer]. Additionally, most of these errors could have been caught if users had checked the computed results with simple hand calculations early in the process. Cases have also been shown where several expert finite element engineers solved the same problem with various FEA software packages and received greatly different results [Symonds].

While trusting incorrect results is clearly an issue to be considered, the question still remains as to how best to approach this problem. One way in which to do this is through validation of the results by comparing them to other analyses rather than treating them as standalone fact. One way of doing this is through preliminary hand calculations

or mathematical models. Oftentimes, a user can estimate a range that the result should fall in. Another way is through the use of prototypes. Building physical models of the system and testing them is a great way to validate the results of a study.

It is also important to remember the iterative nature of the FEA process. When beginning to solve a problem, the user should never approach the first attempt as an actual solution. Simplifying the problem to its very basic level can help the user understand how the model and all its components work together to provide a solution. The user can then manipulate the inputs, even one at a time, to understand exactly how they affect the solution. Building the model in this step by step manner is a great way to help understand the components of a model, to better verify they are working together in the manner that the user wants. The key to a successful finite element study is challenging and understanding the transition and assumptions between each stage of the model, rather than accepting the results as a “ready-to-go report” [Conover]

Clearly, FEA tools are quite powerful. However, in this power lay the danger of misusing the results. In general, an FEA user should always remember that any analysis software is based on theory and approximation which can be pushed beyond its range of validity [Smith].



## CHAPTER II

### **Modeling and Analysis for the Adaptive Vehicle Make**

#### 1. AVM Background

As the complexity of modern technology continues to increase, the time it takes to design and verify systems which integrate these complex technologies is increasing rapidly [Wiedenman]. In an effort to combat these challenges in design and production time, the Defense Advanced Research Projects Agency (DARPA) has invested in Adaptive Vehicle Make (AVM) research. These research efforts aim to revolutionize the design, verification, and manufacturing of systems, particularly complex defense systems and vehicles, to decrease production time by a factor of 5 [Wiedenman].

There are several reasons for increases in design time as system complexity increases. One is that it is often difficult to understand how something works before it is actually built. Another is that complex systems are designed using subsystems, which oftentimes have trouble interacting with each other without failure. A third is that only so many brains can be working on one part at a time. The AVM project seeks to address each of these roadblocks to lead to shorter design times.

The three main projects in the AVM portfolio are META, iFab, and FANG. The META project is a design tool that acts as an aid to compositional design synthesis. Its main focus is to help designers understand how something works before it is actually built. The iFab project focuses on the manufacturing side of system development, and is exploring ways to get away from the straight line manufacturing model and go towards

more of a network of manufacturing capabilities which are programmed and used as needed. FANG addresses the issue of how to get more brains involved to collaborate on a design effort. FANG looks at crowd sourcing, in which the global “crowd” of everyone in the world may have access to design tools, such as the META platform, in order to work together on a design, with the idea that a team of people will almost always have better ideas than an individual [Adaptive].

A closer look at the META project reveals that it is a research initiative aimed at developing a cyber-physical modeling language. The META software tools possess a large bank of CAD models of various components used in a generic system. The user can select various design parameters for the desired system, and the software helps iterate through different combinations of components in order to choose a design that fits all the parameters and is optimized for performance. The analysis and optimization portion of this process is done using various techniques, ranging from simple calculations to complex finite element simulations.

The META project is the portion of the AVM program in which finite element tools can have the most impact. The same issues that exist for individual studies also exist for the META project, such as failure identification, integrating optimization, and solution validation. The following examples show ways in which others have dealt with these same problems.

The DARPA META team published a report in September of 2011 at the Palo Alto Research Center summarizing a year of work on the project. As discussed, the project aims at compressing the product development and deployment timeline for complex military systems. META focuses on developing a model based system

engineering framework to enable architectural analysis of systems during the conceptual design phase, allowing the user to make cost-saving, safety-enhancing decisions from an early point in time [Johnson]. The report discusses the development of the component library, design space exploration method, and failure identification. The report then discusses the successful implementation and verification of the process on the ADAPT EPS testbed and the Ramp System of an Infantry Fighting Vehicle. [Johnson]

Attempts at this style of design have been made in the past. In 1998, Nagler published a paper on using commercial simulation tools (CAD, FEA, a high description language-analog network, and a visualization tool) to aid in the design of microelectromechanical systems (MEMS). Nagler recognized that the time-to-market of products in the automotive industry was decreasing rapidly thanks to the then recent developments of CAD tools, and that integrating FEA tools into an automated design loop would allow for continuous design optimization, with the overall goal of decreasing manufacturing time by integrating all phases of design and optimization into one system [Nagler], a similar goal and plan to that of the AVM project.

Additionally, works have been published regarding identification of functional failure points early in the design process. Identification of failure points is one of the keys to successful design, and is important in attempts to shorten the design cycle. Kurtoglu published a paper in 2010 detailing a simulation-based failure analysis tool which analyzes failures and their propagation to allow system level architectural designers to make decisions based on risk on a functional level before specific components are selected [Kurtoglu].

In the past 15 years since Nagler's paper was published, huge advances have been made in CAD and FEA software and in computing power. In 2011, Rai and his team presented a paper on simulation-based design of electrical power systems on an aircraft. Working with the META program, Rai discusses how as the complexity of modern systems continues to increase, the relationships between subcomponents becomes more complicated and increasingly non-linear. Therefore, exploring the design space during the conceptual phase can help ensure that subcomponents mesh together to prevent disaster while allowing for the greatest flexibility to explore design alternatives when looked at from a high level. A framework for this simulation-based design in Modelica is presented, with results suggesting that successful trade-off studies be performed before costly design decisions are made [Rai]. Again, this sort of early design space exploration using finite element tools is an emerging and effective trend in design.

The advances in computing power and simulation programs, coupled with an increased demand for highly complicated systems to be designed in short amounts of times, makes advances in design even more important and feasible. Other groups around the world are working on similar sorts of tasks. As discussed, changing the design cycle, particularly at a high level when still exploring different design architectures, can save time, money, and resources when done correctly.

A large challenge of the AVM project is the coding side of the problem in getting all of the modules to work together and speak to each other, mainly done by computer and electrical engineers. However, the mechanical challenge comes in setting up the design and analysis interfaces. Traditionally, both design and analysis take huge amounts of human reasoning and intuition. Simplifying this into a process that can be run by a

computer is difficult. One of the hardest parts of analysis comes in knowing how to interpret results of a study. As evidenced by the following studies, much care must be taken in selecting realistic input conditions and in evaluating results, which can oftentimes be unrealistic. This challenge provides the main motivation behind the following studies, which all detail common physical phenomenon, providing a basis on which to compare the simulation results to actual occurrences in the physical world. Understanding what takeaways can be had from a finite element study will then help in taking steps toward in improving the design process with FEA tools.

As mentioned previously, design, in any circumstance, is always an iterative loop of new design followed by analysis and then back to design. The designer has a concept in mind, builds some sort of prototype of this concept, and then analyzes the prototype to see where it can be improved upon. This iterative loop is where finite element analysis software can be most helpful. One of the overall goals of the AVM project is to make this iterative design loop as “smart” as possible using a database of CAD parts and a finite element tool. The parts are modeled and then imported into the analysis tool. The results of the studies performed can then help make design decisions and determine which features of a part are redundant and can be eliminated, and which need to be improved or redesigned, as well as how the different parts of a system interact when together.

One of the ways to demonstrate the META tool and the AVM model is to apply it to an actual, smaller scale engineering problem. One of the advantages of this is that the model of the system can be physically present. All of the parts, their dimensions, weights, and material properties can be readily available for smaller systems. It is, therefore, easy to take measurements and create an accurate model of the system and phenomenon

involved. In addition to the modeling advantages, having the physical system present also helps in validating the results, the second goal of this project.

An initial system under consideration for these studies is a 1/5<sup>th</sup> scale model of an actual racing truck, the Baja 5sc Super Sport remote control vehicle made by HPI Racing [Baja]. This vehicle is run on a 2.9 horsepower engine. Many of the important power train components or specialized pieces are aluminum, but a large portion of the vehicle is plastic, particularly many of the structural components. The vehicle is close to 3 feet in length and is capable of moving at speeds up to 40 miles per hour. This vehicle has all the capabilities and characteristics of a full sized vehicle, but is scaled down so that it is more manageable to model and understand, making it the perfect vehicle for this project.

Two main parts were identified as good candidates for study using the FEA tool. The first was the main chassis of the vehicle. The chassis is the most important structural component of the vehicle, and houses the vehicle's engine and key power train components. Failure in the chassis would be catastrophic to the vehicle.

The second key component that was selected for study was the front bumper of the vehicle. The front bumper is designed to absorb a majority of the force applied from any sort of collision that the vehicle could undergo. The front bumper has to be rigid enough to deflect any sort of load from small scale collisions, but also must have the ability to absorb much of the load in large collisions, such that the body of the vehicle remains unharmed.

An image of the vehicle with the two parts that were studied identified is shown below.



Figure 1: Vehicle with Chassis and Bumper Locations Labeled

The following sections will detail the modeling, various types of analysis, and results from the finite element studies for the two parts being considered. The ANSYS program will be used for all finite element analysis [ANSYS]. These studies, although not extremely complex, provide good examples of studies that would actually be done in industry, and may factor in to the iterative design loop of the vehicle. Upon conclusion, it will be determined how using these results could help to optimize design from a top down level.

## 2. Main Chassis

The main chassis component is the most important structural member of the vehicle. Located in the center of the vehicle, the main chassis houses several key power train components, and also serves as a connection between the front and rear bulkheads of the vehicle. The chassis, like most structural members, is subject to many loads, both

structural and thermal. It provides a good part for analysis as these loads are often predictable and quantifiable.

The first step in analyzing a system is to create an accurate model of the parts involved. The main chassis was first modeled in the CAD tool, with the resulting geometry shown below. This geometry can then be easily imported into the FEA tool and edited as necessary. However, in general, are FEA tools are not used as an geometry editing tools due to the limitations of the programs and the strong CAD softwares available. The main chassis CAD model is shown below, with the front of the vehicle on the right.

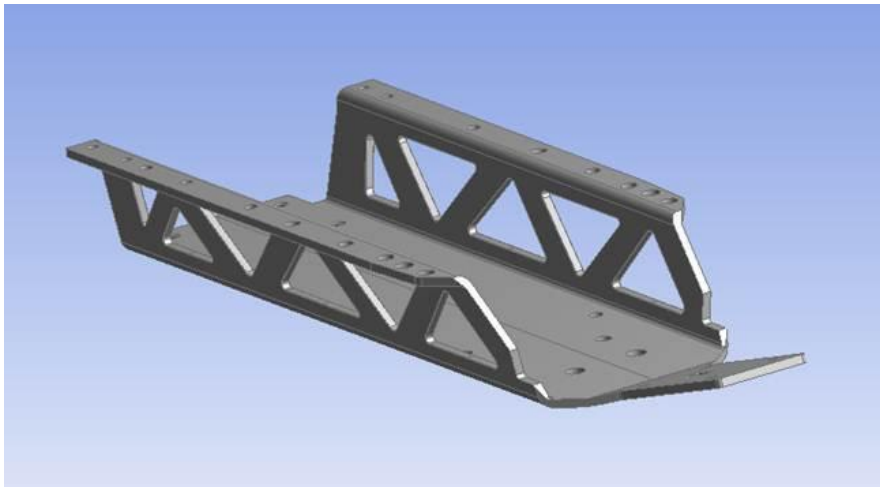


Figure 2: Main Chassis CAD Geometry

The next step was to input the engineering data. FEA tools are equipped with a large library of materials and their engineering properties and characteristics. The user has the option to use one of the preset materials with all of the properties included or to create a new material with custom properties input by the user. Most typical structural



components are included in the general materials section of the database, and any particular materials can generally be found in the explicit materials section. The main chassis part that is under consideration is aluminum, and for the purposes of this study, the “Aluminum Alloy” material properties will be used, with a density of  $\rho = 2770 \text{ kg/m}^3$ , Young’s Modulus of  $E = 71 \text{ GPa}$ , and Poisson’s Ratio  $\nu = 0.33$ .

After inputting the geometry and material characteristics into the model, the next step was to run the analysis. For the main chassis part, three different types of studies were run: static structural, modal, and thermal. These studies will be discussed in detail below.

### *2.1 Static Structural Study*

The first study to be performed was a static structural study. This type of study allows the user to input all supports and loads acting on a body. The solver can then determine the resulting stress, strain, and deformation of the body at a particular point, in a particular direction, or across the body as a whole. This type of study is very useful in solving simple statics problems on complicated geometries, and does well in showing where the highest values of stress and deformation occur on the body, which are the most likely points of failure. It can then be determined whether the part will fail, and what the factor of safety is at various points on the model. This type of study is necessary for all structural members, chassis in particular, to help determine whether or not the structure will fail and how to improve the design either from a strength standpoint or in reducing the cost and weight of the structure.

Upon opening the finite element tool ANSYS, the first step was to assign a material to the geometry. This was done by simply selecting the aluminum alloy that was preselected in the engineering data section. The next step was to generate a mesh for the model. A fairly fine mesh with a relevance, corresponding to the coarseness or fineness of the mesh, of 100 was selected.

Next, the loads and supports were added to the model. To do this, the chassis had to be viewed independently of all other structural members, to isolate the external forces acting on the body. A good way to do this was to imagine a simple free body diagram of the chassis. The sum of the forces on the body has to be equal to zero for a static object. Therefore, the sum of the supports acting in directions opposite of the applied loads has to be equal to the sum of the applied loads in order to have a statically stable system. In this case, all of the loading on the chassis acts downward on the base plate of the chassis, and the chassis is supported at the two raised flaps where it connects to other structural members. The support was modeled as a fixed support on the two underneath surfaces of the flaps. The loads were slightly harder to characterize, but were also very important to the integrity of the study, as incorrect loading can greatly affect the results in a negative way. From the manufacturers data as well as physical measurements of the weights of several vehicle components, it was determined that the load on the chassis should be divided into two forces [Baja]. The first was a 150 N force distributed over the surface of the base of the chassis to account mainly for engine weight as well as other connections and parts. The second was a 50 N force acting at the four holes in the necked portion of the chassis, acting in the negative z direction (downward). The two forces were both conservatively high, and accounted for the static load of the vehicle under normal

operating conditions. A figure showing the chassis with the fixed support and applied forces is below.

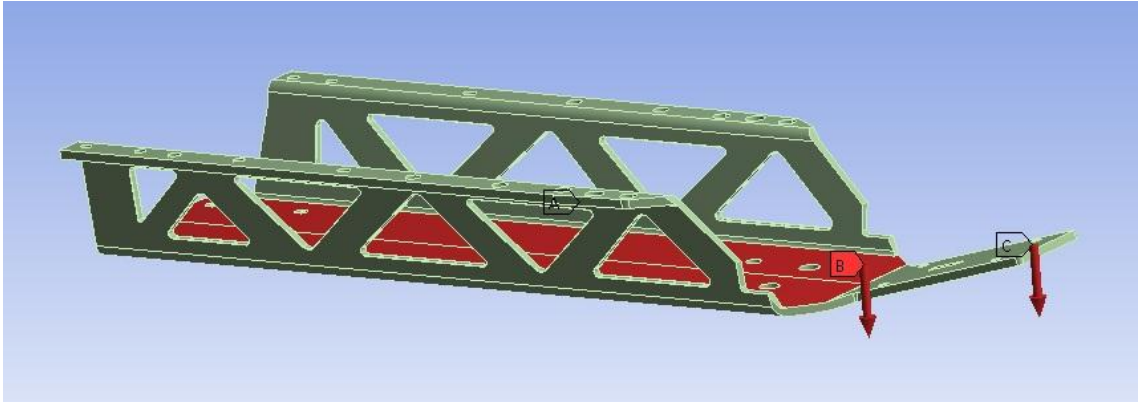


Figure 3: Chassis Loads and Supports

Once the loads and supports had been specified, the solution information, or desired results, had to be determined. For this type of study, it is helpful to determine the Von-Mises Stress across the entire body to see where areas of maximum stress occurred. The total deformation is also important to consider as it helps determine if the deformation will affect vehicle operation at all or if it can be neglected. Finally, the factor of safety will also need to be determined to see how close the part is to failing. These three pieces of solution information were requested, and the model was complete.

After inputting all of the loads, supports, boundary conditions, and solving criterion, the problem was solved. A first pass at the solution revealed that the results around the holes in the chassis for bolts and other connections were not very refined, and some stress concentrations were noticeable. This was likely due to the relatively coarse mesh around the holes. To resolve this problem, mesh refinements were added on the

edges around the holes to increase the number of elements and nodes, making the mesh finer and yielding more realistic results. Refinements were also used around the narrower neck section of the chassis to increase the fidelity of the solution in an area of critical stress and strain.

With the refined mesh, the solution showed a much higher resolution. A figure showing the resulting stress distribution is below. Important things to note are the maximum stress value of roughly 67 MPa, occurring at the edge of the region where the necking in the chassis occurs. This stress concentration was to be expected, as the load on the neck acting at a distance from the fixed supports creates a moment arm causing a bending stress on the neck region. The bending stress causes a tensile stress on the top face of the chassis and a compressive stress on the bottom face. However, maximum stress must always be considered relative to the ultimate tensile strength of the material. Aluminum's tensile strength is around 300 MPa, so even at the point of maximum stress, the part still has a factor of safety of 4.2.

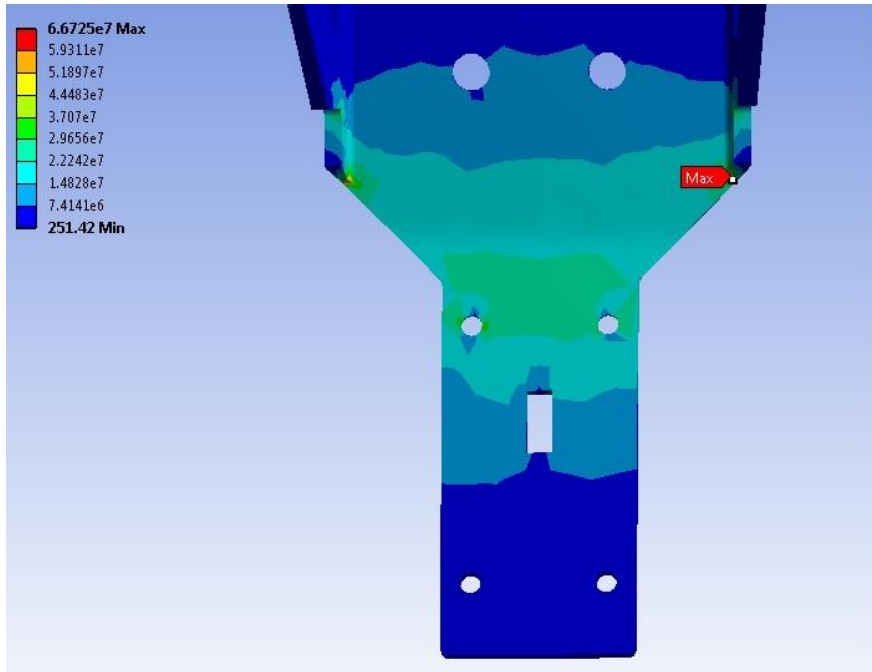


Figure 4: Chassis Stress (MPa)

The other result to consider was the deformation of the chassis. Excessive deformation could have very negative effects on the overall structure of the vehicle. The study showed a maximum deformation of only 1.1 mm at the very edge of the neck of the chassis. This small amount of deformation is negligible, and will have no effect on the structural stability of the vehicle.

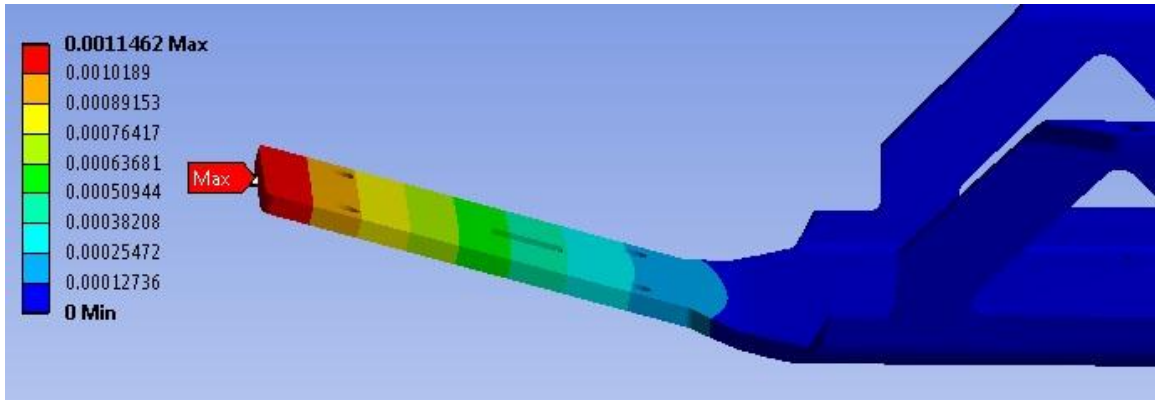


Figure 5: Chassis Deformation (meters)

As mentioned earlier, the most important part of a finite element study is oftentimes not the results, but rather the takeaways from the results. The maximum stress on the chassis was calculated to be 67 MPa. However, that, in no way, means that the part will never experience more than 67 MPa. In a dynamic loading environment such as a vehicle, the applied loads are constantly fluctuating as the mass of the vehicle faces a variety of accelerations from different operating conditions. In this case, the loading values were selected conservatively and the part still maintained a factor of safety of over 4.2, so it is safe to say the chassis will not fail.

In terms of a redesign, the analysis has helped to identify the weakest area of the chassis which, although it is structurally sound, should not be tampered with too much. The main part of the chassis, however, where the fixed supports are, has a factor of safety of greater than 15 throughout. This strength comes from the triangular truss structure of the side supports, which provide a sufficient load path. In high performance cases where weight is very important and the factor of safety can be lowered, it may make sense to decrease the width of these triangular supports. The analysis has shown that the part will

not fail if significant width and thickness is removed. This ability to redesign and test without creating expensive prototypes and testing procedures is a huge advantage of using finite element analysis.

## *2.2 Modal Vibration Study*

The next study to be performed was a modal frequency analysis. This type of study is capable of determining the lowest resonant frequencies of a part. This is important for all parts which are exposed to a cyclical loading pattern. If the frequency of an applied load to a component gets close to the natural frequency of the part, the load will become amplified and the part may experience extreme stress and deformation, and may potentially fail. Numerous cases of failure have been attributed to resonant frequency loading, as it is sometimes unaccounted for in design. Finite element analysis tools make it fast, easy, and cheap to check the modal frequencies of a part.

For this study, the geometry and engineering data are consistent with the model used in the static structural study. Therefore, a new modal study can be added to the same model, with a link between the geometries of the two studies so that the modal study uses the same CAD geometry file of the main chassis as the static structural study.

For a modal analysis study, the only conditions that need to be applied by the user are the supports. The solver is then able to determine the natural frequencies of the structure. In this case, a fixed support was applied under the two horizontal structural flaps, as in the static structural case. However, unlike the static structural case, where a load was applied to the neck portion where the chassis attaches to the front bulkhead, a support, rather than a load, was applied in this case. This is because the bulkhead applies

the frequency to the chassis, so the two move relatively to each other, and either may be considered fixed to study the dynamics of the other.

After applying and verifying the necessary support conditions, the problem was solved, and the first 4 natural frequencies were found to be 1168.2 Hz, 1640.8 Hz, 1712.6 Hz, and 1911.7 Hz. Images showing the maximum deformation of the chassis at each of these frequencies can be found in [Appendix A]. To check the relevancy of these results, the frequencies that the chassis will be exposed to had to be determined.

The chassis is subject to two main vibration loads during vehicle operation. The first is the frequency applied by the terrain on the vehicle. For example, if the vehicle is traveling on gravel, the applied frequency could be as much as 30 to 50 Hz. This frequency, although small, could potentially have impact. The other applied frequency is due to the engine. The engine used in this vehicle is a Fuelie 26S CC engine which has a maximum rpm of 15,000. This corresponds to an induced frequency calculated using the simple conversion shown below.

$$\frac{15000 \text{ rev}}{\text{min}} * \frac{1 \text{ cycle}}{1 \text{ rev}} * \frac{1 \text{ minute}}{60 \text{ seconds}} = 250 \text{ Hz}$$

The two applied frequencies are therefore roughly 40 Hz and 250 Hz. The modal study in ANSYS gave a minimal natural frequency of 1168 Hz, more than four times the maximum applied frequency. These results suggest that the chassis is designed such that the resonant frequency is not a factor, implying a good design. Resonant frequency can be a concern on some parts which are thinner or have a smaller stiffness, and should therefore always be considered. There are several ways to redesign a component to



change its natural frequency, including changing the thickness of structural elements or adding support members to the component to change the stiffness.

### *2.3 Thermal Study*

The third and final study performed on the chassis was a thermal study. Thermal studies are important in scenarios involving large amounts of heat being generated that need to be dissipated. The important case to consider with a thermal study, as with any study, is the worst case scenario. In the case of this vehicle, the engine produces a majority of the heat due to the engine combustion and frictional losses of the internal components of the engine. The engine sits directly on the chassis, so it can be assumed that a portion of the heat generated will flow to the chassis through conduction. From there, the heat is dissipated out through the chassis to other structural members, as well as to the air moving past the vehicle in the form of convection.

The first step in modeling this thermal scenario was to determine how much heat energy the engine was producing. From the manufacturer's data [Baja], the engine is capable of producing 2.9 horsepower of power, or 2160 Watts. This means that the engine shaft output is 2160 W. However, much more energy had to be consumed in order to overcome the losses of the engine, as no engine has an efficiency of 100 percent. The engine efficiency suggests that 30 percent of the energy produced is actually transmitted to the shaft as mechanical energy, meaning the other 70 percent is lost as heat. Therefore, for every 2160 W of mechanical energy produced, 5040 W of heat is produced. Of this 5040 W, only about 10 percent is actually transferred to the chassis, due to high rates of convection. This calculation is shown below.

$$2.9 \text{ hp} * \frac{745.7 \text{ W}}{1 \text{ hp}} = 2160 \text{ W} * \frac{70}{30} = 5040 \text{ W} * 0.1 = 504 \text{ W}$$

Therefore, a conservative estimate of 500 W of heat energy is transferred to the chassis during maximum operating conditions. Although conservative, this load provides a good worst case scenario.

The next step was to determine the dissipation path that this heat would take. The chassis is connected to other structural members, so heat flows to these other members through conduction. However, a large portion of the surface area of the chassis is also not touching anything and is exposed to the surrounding air. Heat will be transferred through convection from these surfaces to the surrounding air. Stagnant air is a good thermal insulator, while moving air conducts heat well. Therefore, there will be a great difference in the heat transferred from the chassis when the vehicle is in motion as opposed to when it is at rest. The case being modeled is a worst case scenario, in which the heat produced is a maximum and the engine is at full throttle. This occurs when the vehicle is moving at top speed, and can be associated with high rates of convection. Therefore for this study, convection is the dominant form of heat transfer, and conduction to other structural members can be neglected.

To quantify this convection, the heat transfer coefficient (h) and the ambient temperature must be known. These can be assumed to be  $h = 150 \text{ W/m}^2\text{K}$  and  $T_{\text{amb}} = 22 \text{ }^\circ\text{C}$ , based off data found in heat transfer tables for moving air [Kays].

Once these physical phenomena were quantified, the next step was to put this data into the finite element tool. As with the modal analysis case, the thermal study also uses the same geometry, mesh, and material properties as the static structural analysis. Since the scenario is worst case, a steady state thermal analysis was used, as the heat load will not fluctuate from the maximum possible load. The two external conditions that need to be applied are the heat flow into the chassis from the engine, and the convection of heat out of the chassis to the surrounding air. As discussed above, a 500 W heat load was applied to the base face of the chassis, and convection with a heat transfer coefficient of  $150 \text{ W/m}^2\text{K}$  was applied to all faces of the body. The desired solution information of the temperature profile of the entire body was requested, and the problem was ready for solving.

The heat transfer problem was solved, and the resulting temperature profile is shown below, with temperatures given in degrees Celsius. The maximum temperature was found to be  $78^\circ\text{C}$  in the middle of the base of the chassis, with the minimum temperature of  $28^\circ\text{C}$  located at the edge of the neck portion of the chassis.

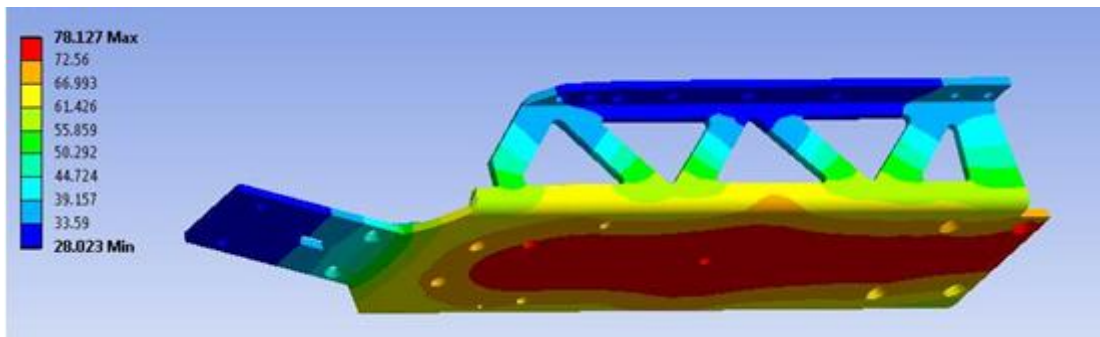


Figure 6: Chassis Temperature Profile ( $^\circ\text{C}$ )

These results are only estimates, but they provide worst case estimates which are helpful in analyzing the design. 78 °C is well below the melting point of aluminum, so failure is not an issue. The bigger concern is safety of the user as they interact with the vehicle. 78 °C is hot to the touch for an adult, but will not burn an adult as long as they remove their hand quickly. Although safe for careful adults, this high temperature could cause injury to a child, so this vehicle is not safe for children, nor was it designed to be a child's toy. The range of temperatures from 78 °C to 28 °C suggests the chassis does a good job of dispersing the heat with its large surface area, ensuring that the parts of the chassis that are in contact with other members, such as the neck connection to the front bulkhead, do not get too hot. Overall, the chassis serves its purpose of distributing the heat from the engine while not getting too much hotter than safe operating conditions should allow.

### 3. Front Bumper

The next part to be analyzed was the front bumper, another important structural member located at the front of the vehicle designed to protect the vehicle from damage due to collision. The bumper is unique in that it does not have much static load, and should, ideally, never have to take a load from a collision. However, in the case of a collision, the bumper must deform such that it absorbs most of the force without damaging the rest of the vehicle.

As with the main chassis, the first step in a finite element analysis is to model the geometry. For the front bumper, the part was modeled with the CAD tool and imported into the geometry section of the FEA tool. The model of the part is shown below.

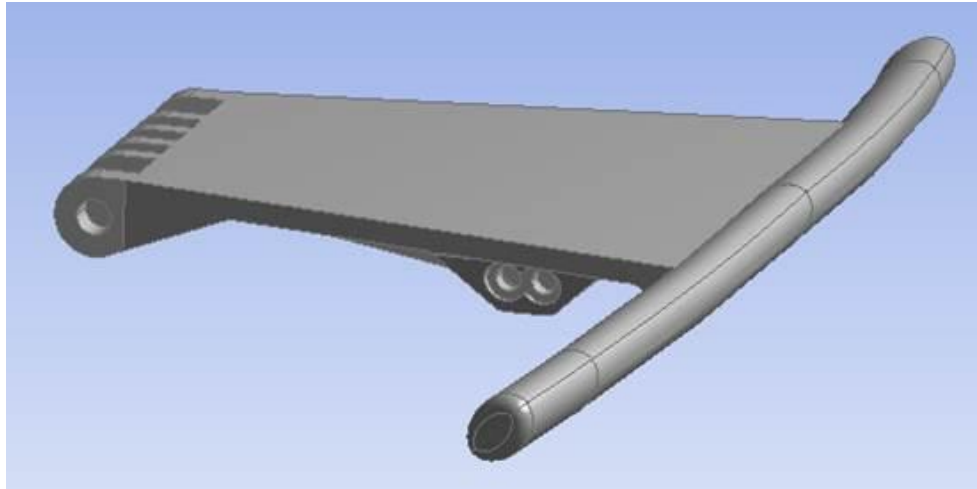


Figure 7: Front Bumper CAD Geometry

The next step in the ANSYS process was to input the engineering data and material properties. Although the chassis was made of aluminum, the bumper is made of plastic, which is more difficult to characterize. To achieve the desired material properties, a modified version of polyethylene was used. A generic material was selected as a base, and then certain characteristics were changed. In this case, Young's modulus ( $E$ ) is known to be 1.1 GPa, Poisson's ratio ( $\nu$ ) is 0.4, and the density ( $\rho$ ) is  $960 \text{ kg/m}^3$  from manufacturer data. This information was entered to create the correct material for the front bumper.

The front bumper is also unlike the chassis in that it does not experience any important thermal or static loading. The main two loads that a front bumper would face are the induced vibration from the motion of the vehicle and the impact load should the vehicle come in contact with any other objects. Therefore, the two studies that were performed were an impact study and a modal analysis.

### *3.1 Impact Study*

The first study to be considered was an impact study, designed to see how the bumper would react to different collision scenarios. This study was modeled using a static structural analysis in the ANSYS finite element analysis tool.

The first step was to assign a material to the geometry. The modified polyethylene was selected for the entire body using the material properties listed above. The next step was to mesh the part to ensure that the mesh was fine enough for a realistic analysis. The mesh relevance was increased to 100, and a refinement was added on the front edge of the bumper to handle the higher stress concentrations.

The next step was to assign all of the loading and support constraints to the model. The supports in this case were fairly straightforward. The front bumper is rigidly connected to the other structural members by fasteners through holes along three different parallel axes. A fixed support was added on the faces of each of these holes to rigidly fix the bumper to the rest of the vehicle.

The loads for this model were slightly more complicated. Two types of collisions were considered. The first is a “fender bender” type scenario. For this case, the vehicle would be traveling around 3 m/s, a typical speed for slow vehicle operation. The front bumper of the vehicle would then come into contact with an object (wall, tree, etc.), decelerating the vehicle to 0 m/s in roughly 0.2 seconds. The resulting calculated acceleration can then be used to determine the force exerted to achieve this acceleration for the 20 kg vehicle. The acceleration and force were calculated using the following

equations, in which  $a$  is acceleration,  $v_2$  and  $v_1$  are final and initial velocities respectively,  $t$  is time of collision or impact,  $f$  is force, and  $m$  is mass.

$$a = \frac{v_2 - v_1}{t} = \frac{0 \frac{m}{s} - 3 \frac{m}{s}}{0.2 s} = -15 \frac{m}{s^2}$$

$$F = m * a = 20 kg * -15 \frac{m}{s^2} = 300 N \text{ opposite direction of motion}$$

The front bumper experiences a force of 300 N giving it a negative acceleration of  $15 \text{ m/s}^2$  in a typical slow moving collision for this vehicle. The second case to consider is a worst case scenario type condition, in which the vehicle is traveling at its maximum speed of 20 m/s and collides with an object, forcing it to come to rest in only 0.1 seconds. The resulting acceleration and force calculations are shown below.

$$a = \frac{v_2 - v_1}{t} = \frac{0 \frac{m}{s} - 20 \frac{m}{s}}{0.1 s} = -200 \frac{m}{s^2}$$

$$F = m * a = 20 kg * -200 \frac{m}{s^2} = 4000 N \text{ opposite direction of motion}$$

The second case produces a 4000 N force resulting in a negative acceleration of  $200 \text{ m/s}^2$ . Both the force and acceleration need to be modeled in the software for both the less severe case and worst case scenario.

After assigning the material, generating the mesh, and inputting all of the external conditions, the next step was to solve the problem. This was done for both the less severe case and worst case scenarios. The resulting solution information that was requested was the total deformation of the part, the equivalent stress, and the factor of safety across the entire body. First, we will look at the results for the low velocity case.

The maximum deformation of the bumper was found to be 5.13 mm, occurring at the two outer tips of the bumper. The maximum stress was found to be 23 MPa, occurring where the bumper is attached to the structural connection. This was to be expected, as the sharp corner should create a slight stress concentration. The corresponding factor of safety at this point was 1.09, the lowest across the part.

The half centimeter of deformation is noticeable, yet not catastrophic. The factor of safety greater than one implies that this part should not fail, and all deformation should be elastic deformation. It appears that for this type of collision, the bumper would come close to failure, but would absorb all of the impact and remain intact, protecting the rest of the vehicle, and serving its purpose as a first line of defense. Figures of the deformation and factor of safety for the first case are shown below.



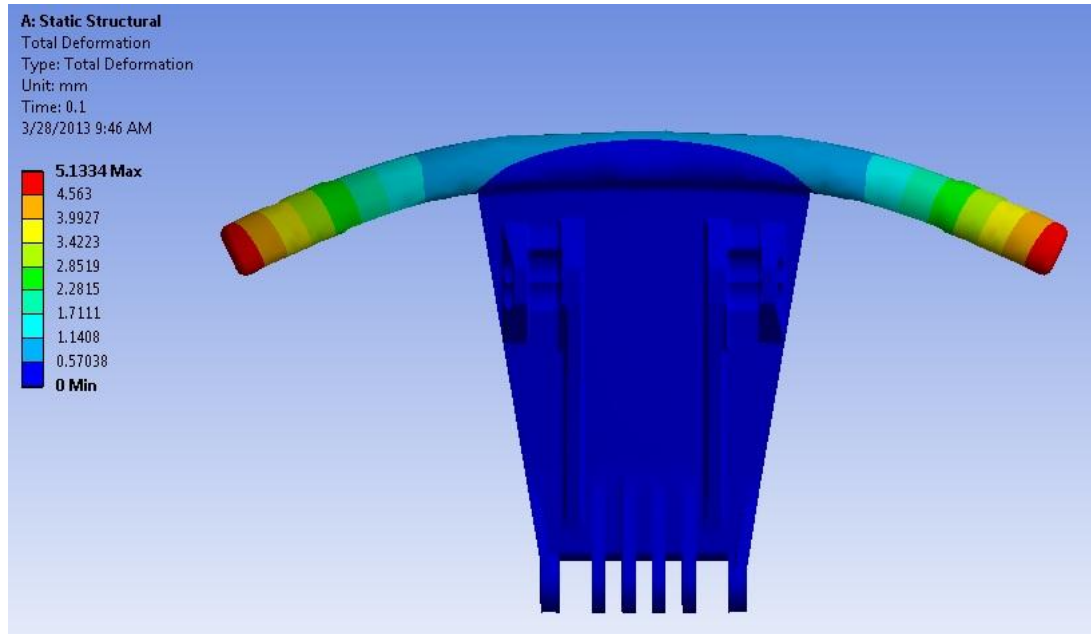


Figure 8: Low Speed Case Bumper Deformation (mm)

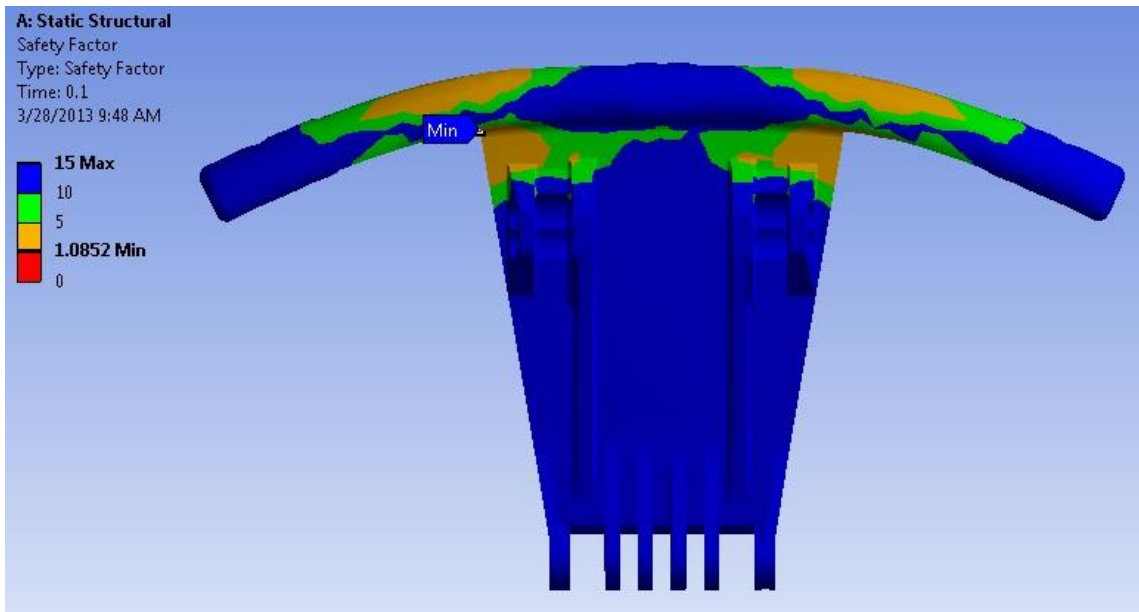


Figure 9: Low Speed Case Bumper Factor of Safety

Next, the results for the worst case scenario collision were studied. Again, the maximum deformation and minimum factor of safety were the two most important pieces of data. The maximum deformation was found to be 67.4 mm, or nearly 7 cm, and the maximum stress was 302 MPa, giving a minimum factor of safety of 0.08. This is clearly a much greater stress than the previous case, and the low factor of safety suggests that this part will certainly fail. The deformation becomes less of a meaningful result therefore, because this plastic part will fracture before it deforms this much. From these results, we can conclude that the bumper will break if the vehicle hits an immovable object at maximum speed. The bumper should absorb much of the load, so although it would need to be replaced, the rest of the vehicle should be still operable. Figures of the deformation and factor of safety for the high speed case are shown below.

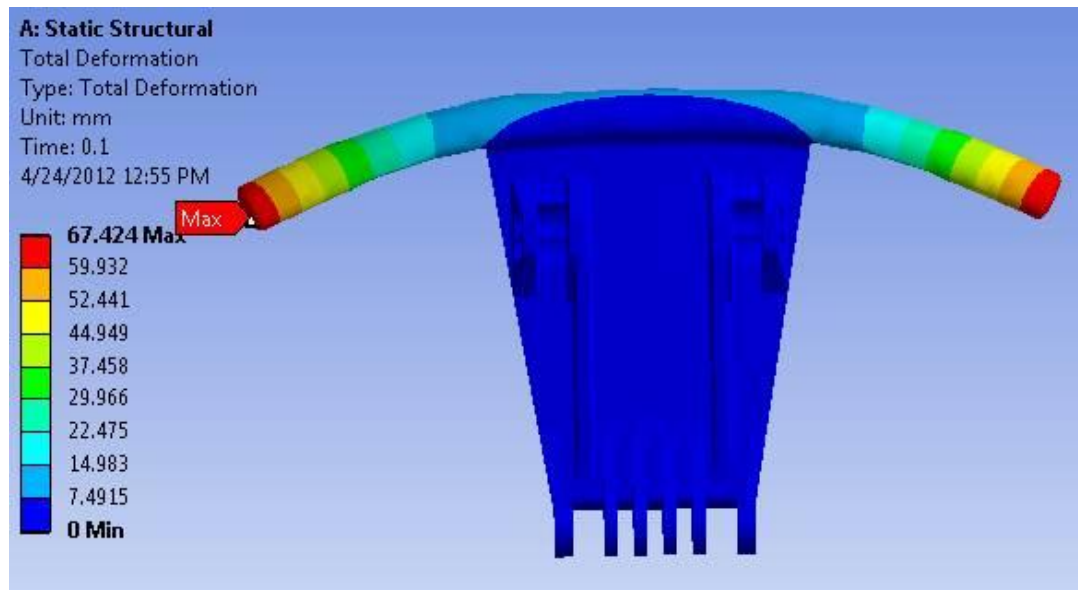


Figure 10: Worst Case Scenario Bumper Deformation (mm)

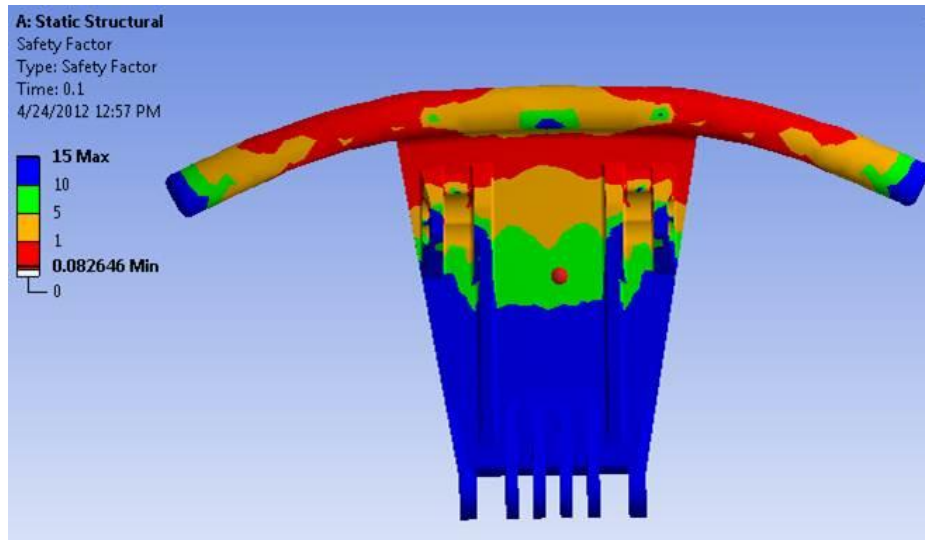


Figure 11: Worst Case Scenario Factor of Safety

After studying and attempting to draw conclusions from these results, the next step was to question how reliable these results are. The biggest weakness with this model was the surface across which the collision force was applied. In the original model, the force acts on the entire surface area of the front bumper, as shown below.

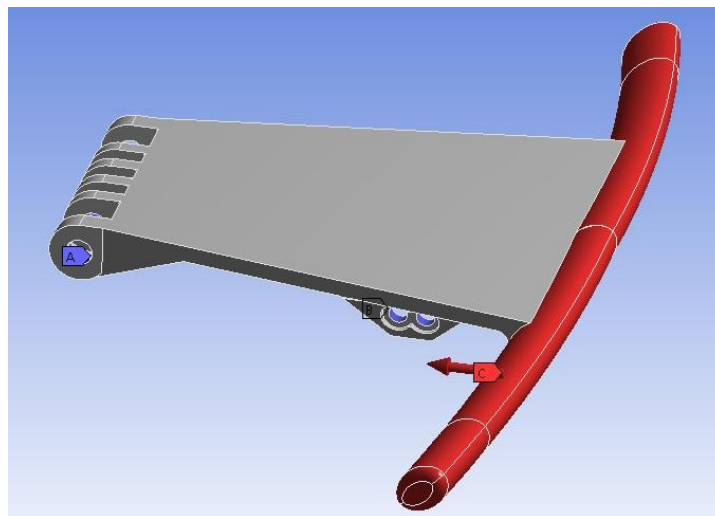


Figure 12: Surface Area of Force Applied to Bumper

In reality, a collision force will almost never act this uniformly. Instead, the load is more likely to occur at one point. If the collision is head on and acts at the center of the bumper, the results are likely to be similar. However, a point load at the tip of the bumper would cause much larger shear and moment forces. The model was changed to replace the distributed load with a point load, as shown below.

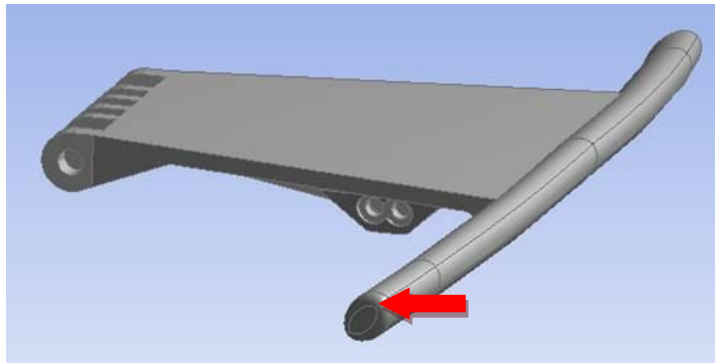


Figure 13: Front Bumper with Point Load

When the low speed case was repeated with the load applied as a point load at one end of the bumper, the results show that the bumper would in fact be likely to fail. A figure showing the factor of safety for this case, with all of the red areas having factors of safety of less than one, is shown below.

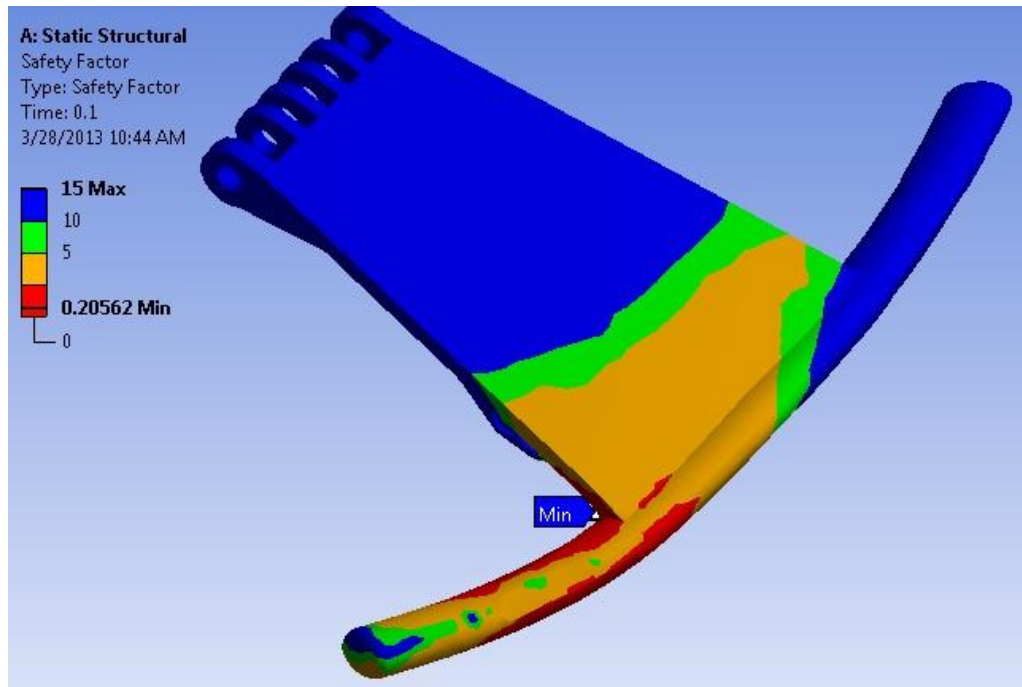


Figure 14: Bumper Factor of Safety Results Updated for Impact Point

Another weakness of this model lies in the boundary conditions at the bolted connections. These connections were assumed to be fixed rigid supports. However, in reality, they are subject to deformation as well, and this could change how the load carries through the vehicle. The model could be improved by studying the entire geometry of the vehicle by importing a large assembly into ANSYS, to see exactly what the load path is. However, studying such a large model would prove to be very computationally expensive. This goes back to the tradeoff between the accuracy of the model and the time it takes to solve the problem, and the balance between these two factors that must be reached for every study. Modeling an entire vehicle may provide slightly more accurate results. However, the solver will solve for the displacement of every node in the entire vehicle, regardless of its proximity to the bumper. In general, it is

best to attempt to isolate the part or section under consideration and provide the most accurate boundary conditions possible to produce results accurate enough to allow the user to draw conclusions.

### *3.2 Modal Vibration Study*

In addition to the impact study, a vibration analysis was also performed. The geometry and material properties were left the same as those used in the static structural study, as the same part is under consideration. As with the chassis, this is easily done by adding links between two studies to preserve geometry and material properties.

As discussed above, the only required constraints for modal analysis are the supports. As in the static structural study, the only supports required are through the bolt holes where the front bumper attaches to the rest of the vehicle. This is where the vibrational frequency is induced, and should be fixed with a support for the purpose of the modal study. The same mesh used in the impact study was also used in the modal analysis.

After applying the fixed supports and updating the mesh, the next step was to solve the problem. ANSYS returned values for the six lowest natural frequencies. These frequencies were 176.15 Hz, 187.16 Hz, 264.81 Hz, 268.41 Hz, 430.89 Hz, and 736.68 Hz. Images showing the modal deformation of the bumper at each of these frequencies can be found in Appendix B.

As mentioned in the chassis analysis, the potential induced frequencies on this vehicle are due to the motor vibrations and the road conditions. Although these are both important to the chassis, the bumper is positioned much farther from the engine, and is

not affected by engine vibrations. Therefore, the only induced frequency is a result of the road conditions.

As discussed above, the maximum frequency from road conditions is generally accepted to be between 30 and 50 Hz on the conservative side. The smallest natural frequency of the bumper is around 176 Hz. This is nearly four times any possible induced frequency, implying that the natural frequency is not of concern. However, if applicable, changes to the design of the front bumper could have been made to ensure a higher natural frequency while still preserving the structural integrity proven in the impact study.

#### 4. Conclusions

Although this selection of analysis only represents a small portion of the possible studies that could be done on this vehicle, many conclusions and important information can be drawn from these studies on the chassis and bumper. First, in a literal sense, from these studies, an engineer can assume that the chassis will not fail structurally or thermally, and has a sufficient factor of safety in both regards. It can also be assumed that neither the chassis nor bumper will be exposed to frequencies close to their natural frequencies. Finally, it can be assumed that the bumper will not fail in some low speed collisions, but is likely to fail in high speed collisions or collisions occurring at certain critical points on the bumper.

These results are the types of conclusions that engineers seek to gain from analysis of components during the design and optimization phase. The important takeaways from these results are the general condition of the part, rather than the specific

numbers. This is an important distinction, and the level of accuracy of the results required directly determines how closely the model must match reality. This is why it is so important to properly define the problem and intended outcome of a study before modeling a problem.

Of the three study types (structural, modal, and thermal), modal is the simplest, and requires the least user inputs. From the studies, it can be concluded that a modal study is a quick, cheap, and effective way to ballpark the natural frequency of a part to see if further analysis must be done. Because of the simplicity of the study, incorrect inputs are less of an issue, and a computer may be capable of automatically performing this analysis with confidence placed in the reliability of the results.

The other two studies (structural and thermal), require much more approximations, estimations of loads, and information from outside sources. A human may use intuition and outside research, as well as a basic understanding of the science involved, to solve the problem as close to accurate as possible. A software program may also be able to make such approximations from tables of experimental data. However, as evidenced by these studies, these results are only as accurate as the approximations that produced them. Being able to make design decisions based off analysis results requires analyzing more than just a maximum or minimum value, but also locations of data points on a component relative to different geometry features, and an understanding of the accuracy and nature of the results.

At a higher level, the literature studied suggests that one of the modern day challenges of engineering is solving the problem of automated system level mechanical design. The challenge, and problem that the AVM project is attempting to address, is the



difference between isolated component behavior and component behavior in a system. The studies performed in this chapter have explored the challenges with making assumptions and approximations in finite element studies, and the importance of putting results into perspective. The studies provided have shown how finite element analysis tools can be used for redesign. The studies have also shown how modularity in components may be achieved, leading to higher level studies performed earlier in the design process, saving both time and money in the design cycle. However, care must be taken to continue to use finite element tools as tools to help guide design decisions rather than as calculators with results automatically taken as fact.

## CHAPTER III

### **Modeling and Analysis of Brushless DC Motor Failure**

#### 1. System Redesign and Motor Background

Methods and techniques for integrating finite element tools into the high level design process have been discussed. In the next sections, a more detailed look at using finite element tools to analyze systems and perform an optimized redesign will be studied.

Advances in the finite element analysis process have made it a great tool to help accelerate and improve the design cycle. There are several examples of researchers and industry professionals who have taken advantage of this tool and are using it in the design cycle. A few interesting examples are highlighted below.

One of the earliest examples of the application of FEA tools dates back to 1965. A multi-material rocket was modeled as an axisymmetric solid with a toroidal ring of triangular cross section. The model was solved for temperature for the heat conduction analysis and radial and axial displacements for the stress analysis [Wilson 1965]. Wilson and his team then used this data to change the original model to incorporate what he had learned from his finite element study into his design. Similarly, numerous modern day examples can be found exemplifying use of finite element optimization tools to change the design of a system. These studies range from the radius of a hole in the middle of a plate to a heat insulating hollow brick wall and even the mass of a truck frame [Singleton], [Coz Diaz], [Yong-hai]. Additionally, examples exist in which the heat

transfer of small electric motors is considered and the conductive and convective effects are studied [Staton 2005, 2008]

Each of these examples uses the finite element method to solve optimization problems. However, one shortcoming in the examples, and the area in which improvement could be made, is that no validation or physical testing was performed to verify the results. Creating prototypes of a system that was optimized using FEA and then testing these prototypes to see if the analytical results are accurate and if the system is, in fact, optimized is an effective way to improve the validity of an FEA study.

One method in which FEA can be used as a tool to aid in the redesign process is through failure analysis. In addition to new design, finite element analysis is also commonly used to analyze systems which have failed to help better understand which part of the system is failing and why. This is an important step in the product development cycle. A redesigned component can then be evaluated and optimized using the finite element software as a design tool.

An example of this type of application is in an electric motor. In particular, brushless motors are often used in advanced, high performance applications where space and weight are a concern, but where a large amount of power and torque is required. For such cases, the high performance requirements often demand large amounts of current. The current, when traveling through the motor coils, produces a large amount of heat given in the equation shown below, in which  $Q$  is heat,  $I$  is current, and  $R$  is resistance [Incropera]. This heat must be dissipated to prevent heat buildup around the coils, which is why heat sinking a motor is so important.

$$Q \propto I^2 * R$$

Due to the space constraints of small brushless motors, it is often difficult to dissipate this heat, as there is sometimes nowhere for the heat to go. One particular type of small brushless motor is a flat motor, which limits the height of the motor to fit a space requirement. Brushless motors generally have circuit boards under the coils to handle the electronic controls associated with the brushless characteristic of the motor. These circuit boards have relatively low thermal conductivities, meaning they allow low amounts of heat to escape from the coils. If too much heat builds up, the motor coil could exceed its maximum temperature, causing the motor to fail. High performance flat motors are not only expensive to replace, but they also may perform vital functions in which failure has severe consequences, as in the case of medical applications.

For one such case, a Maxon EC 244879 flat motor [Appendix C] is occasionally required to run at 3 amps of current for a particular application. However, when run at this load condition for an extended time, the motor is failing due to coil overheating. This is to be expected, as the Maxon motor is not rated to run at such high currents. High current operations increase the temperature of the copper motor coils, which are rated to fail at 125 °C [Appendix C]. The speed versus torque plot for the motor is shown below. In the plot, the red area is rated for continuous operation, while the white area should only be used for short amounts of time. It can be seen that regardless of torque, the motor is not rated for continuous operation at 3 amps.

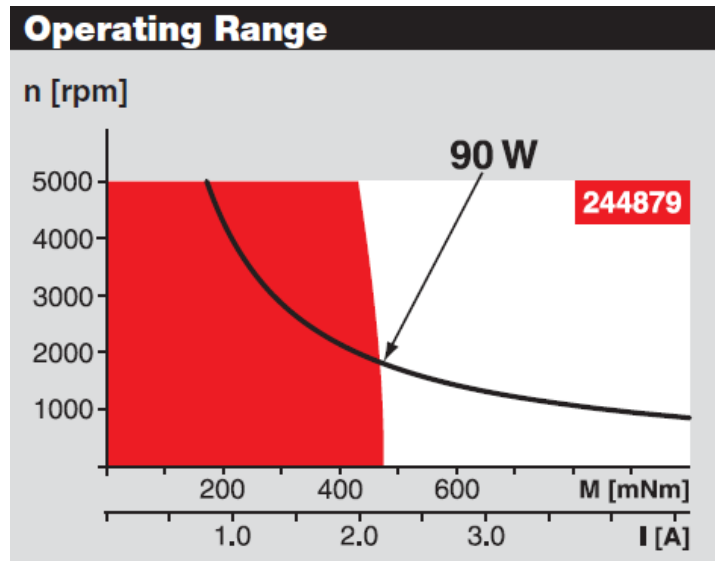


Figure 15: Speed versus Torque Curve for Maxon EC 244879

In this chapter, the motor will be analyzed by creating a finite element thermal model to determine the point and cause of failure. Then, this thermal model will be validated using experimental tests run on the actual motor. Following validation, the model will be studied to determine which modifications can be made to best improve the heat sinking of the motor. Next, these modifications will be implemented into the finite element model and optimized using an optimization sequence in ANSYS. Finally, the optimized modifications will be implemented into the actual flat motor to create a prototype of a motor with improved heat sinking, and the motor will be tested to determine the effect of the modifications. Again, the goal of these studies is to provide one example of the way in which a system can be improved by use of a finite element optimization routine. A picture of the actual flat motor, which will be used as a model for this system, is shown below.



Figure 16: Maxon EC 244879

## 2. Modeling the Motor

As with any study, the first step in analysis was to create an accurate model of the geometry present. This can be done with a CAD modeling package. The motor under consideration was readily available during all phases of this project, which allowed for more accurate modeling, as well as a better understanding of the implications of the results.

This motor had several different components, each of a different material with different material properties. The system was modeled as an assembly of several parts so that each part could be dealt with accordingly in the FEA tool. Creating assemblies with several parts in an FEA tool also allows the user to specify the characteristics at the contact regions of each of the parts. The thermal properties at the interfaces of each of

these parts were important in determining how the heat was dissipated away from the source.

At first glance, this part seemed to be a good candidate for an axisymmetric model. For this type of modeling, a cross section model of the part is rotated a full 360 degrees about the axis of symmetry. This simplification can help by greatly reducing the number of calculations required, saving computational space and time. For the flat motor, an axisymmetric model was considered, but it was determined that it would not work because the motor does not have one solid coil, but rather 18 coils with air gaps in between. These air gaps are important for convection heat transfer, and allow heat to escape tangentially as well as radially from the coils.

The CAD model was created from the ground up, starting with the base and the circuit board, then the stator and coil windings, and finally the magnet and top cover. Care was taken to use exact dimensions, measured using calipers on the actual motor, to ensure accuracy of the model. The base and circuit board were modeled with simple extrudes and revolves. Modeling the stator and coil windings, referred to henceforth as the coils, was more difficult, but also very important, as these elements are the main heat producing and dissipating components. The coils were modeled separately as parts of their own to allow for independent material assignment in the FEA portion of the model. A figure showing the assembled bottom half of the CAD motor next to the actual motor is shown below.

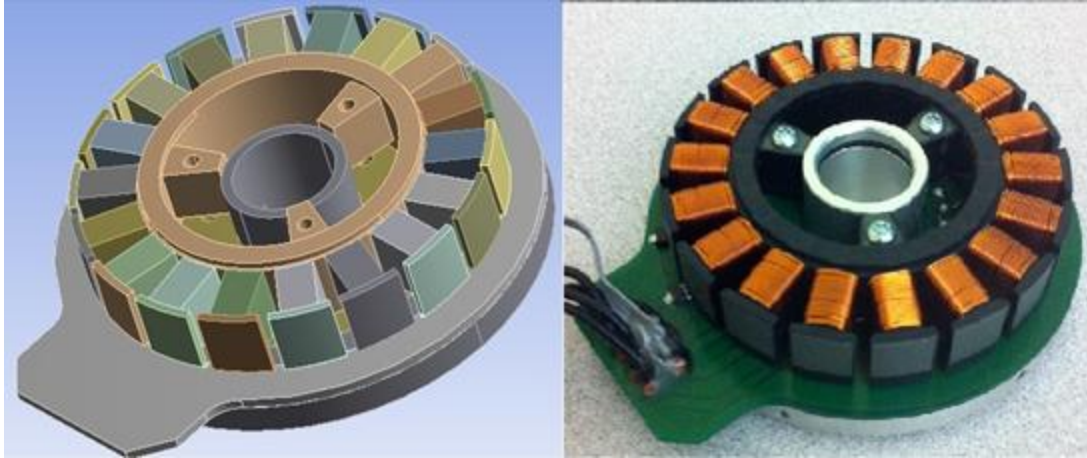


Figure 17: CAD Motor and Actual Motor without Cover

The remaining parts to be modeled were the cover and the magnet, which are placed over the top of the flat motor. These cylindrical parts were modeled with revolves and combined into a sub assembly as they act as one piece made of two different metals “fused” together. This sub assembly was then assembled over the stator and coil, and the CAD model of the motor was complete. The finished geometry is shown side by side with the actual flat motor below.

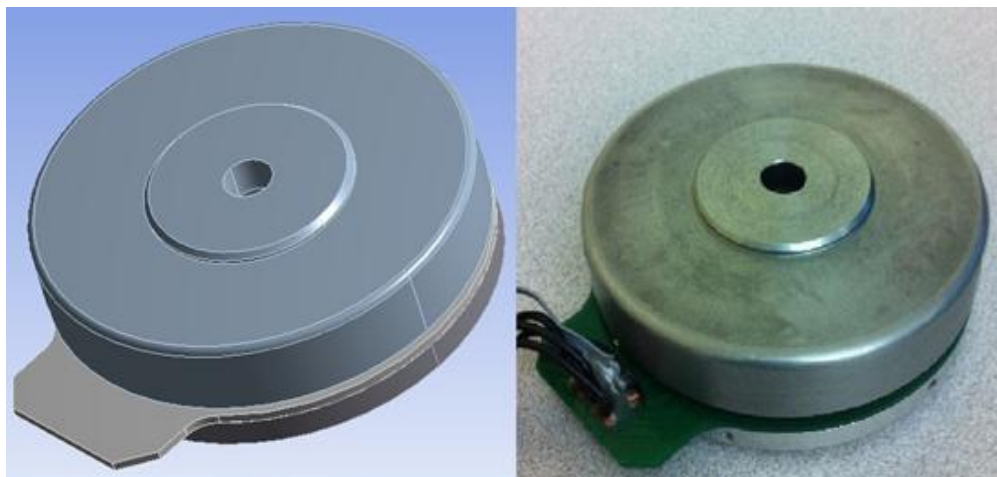


Figure 18: Views of Actual Motor and CAD Motor With and Without Cover



### 3. FEA Study

As mentioned before, the goal of this FEA study was twofold. First, an accurate model of the system had to be created and verified to understand the heat paths and thermal tendencies. Heat-sinking modifications could then be considered in the FEA model and finally tested and verified on the actual motor. As mentioned, the motor coils are rated to fail at 125 °C, which occasionally occurs when the motor in the prosthetic is run at 3 Amps, which is greater than the 2.12 Amps that the motor is rated for [Appendix C]. Rather than try to model the complicated prosthetic system including bearings, shaft, complicated convection currents, and heat sink grease, a simplified system was considered. The motor was studied without the cover, which would normally be rotating, creating complicated forced convection, and without any other boundary conditions such as heat sinks or insulators. The first step in the redesign process is to confirm that these simplifications are valid by verifying the baseline finite element model with experimental tests.

After modeling the geometry, the next step was to begin the finite element analysis. The geometry was first imported from the CAD tool to the FEA tool using the DesignModeler interface. For the first phase of this analysis, the model was studied as built to gain an understanding of the failure of the coils due to overheating. The next phase will attempt to redesign the motor, so DesignModeler must be used to change the geometry for the optimization study. However, for now, the imported geometry will be studied unchanged, and no edits need to be made.

### 3.1 Inputs

As in other studies, the first step was to choose the correct materials necessary for the model. In the case of a thermal study, the only material property required is the thermal conductivity of the material,  $\kappa$ . In addition to conduction, the other types of heat transfer are convection and radiation. Convection will be discussed later, as that is more of an environmental characteristic rather than a material characteristic. Radiation is a function of the Stefan-Boltzman constant,  $\sigma$ , the emissivity of the object,  $\varepsilon$  (1 for a black body), and the area and absolute temperature of the body compared to the absolute temperature of the environment. A rough estimate of the magnitude of conduction and radiation can be calculated to determine which of the two, if either, can potentially be neglected. The equations for the two types of heat transfer are shown below [Incropera].

$$Q_{cond} = \kappa * A * \Delta T$$

$$Q_{rad} = \varepsilon * \sigma * A * (T_{obj}^4 - T_{surr}^4)$$

For the characteristic area, a rough surface area of  $100 \text{ cm}^2$  can be assumed, which will cancel out of the two equations regardless.  $\sigma$  is a constant  $5.67 * 10^{-8} \text{ W/m}^2\text{K}^4$ , and  $\kappa$  for aluminum is  $155 \text{ W/m}^2\text{K}$ . The emissivity of the body will be conservatively assumed to be 1. The temperature of the body can be estimated at around 375 K, noting that order of magnitude is more important using an exact value, with the surroundings at around 300 K, for a  $\Delta T$  of 75 K. The resulting calculation is shown below.

$$Q_{cond} = 155 \frac{W}{m^2 K} * 0.01 m^2 * 75 K \approx 115 W$$

$$Q_{rad} = 1 * 5.67 * 10^{-8} \frac{W}{m^2 K^4} * 0.01 m^2 * (375^4 - 300^4) \approx 7 W$$

Therefore, even with a perfect black body emitter, the heat transferred due to radiation is less than 6 percent of the heat transferred due to conduction, so the radiation effect can be reasonably neglected.

Because only the thermal conductivity is required, it is easy to create or edit materials in the material database as necessary. From inspection of the motor, the base and cover are both aluminum, which has a varying thermal conductivity dependent on the temperature of the aluminum. This data is all programmed, so simply selecting the aluminum alloy will account for the changes in thermal conductivity as temperature varies. The coils in the windings of the motor are modeled as copper wire. Copper has a very high thermal conductivity of 401 W/mK [Arpaci]. The 18 small magnets on the outside of the coils, as well as the magnet on the rotor, have a thermal conductivity of 100 W/mK, modeled as cobalt with a specified thermal conductance [Arpaci]. The housing on the inside of the coils, separating the coils from the rotating shaft, has a thermal conductivity of 80 W/mK, modeled as modified polyethylene [Arpaci]. The final remaining material was the circuit board.

The circuit board is the most complicated to model, as it is not one homogeneous material, but rather an electrically non-conductive substrate etched with copper pathways to carry electric current. The substrate is not only an electric insulator, but also a thermal

insulator, while the copper conducts heat and electricity very well. Clearly, this behavior suggests that the copper pathways allow the circuit board to conduct heat very well in the plane of the etchings, but not well at all through the board. In the scope of the circuit board for this motor, there are fewer etchings than the typical computer circuit board, and we are mainly concerned with the heat traveling through the board and into the aluminum. Therefore, the thermal conductance of the circuit board will be assumed to be 0.27 W/mK, representing heat transferred through the plane of the board [Arpaci]. The material properties of the model are summarized in a table below.

<b>Component</b>	<b>Thermal Conductivity (W/mK)</b>
Base	155
Circuit Board	0.27
Coils	401
Magnets	100
Housing	80
Cover	155

Table 1: Motor Component Thermal Properties

The next step was to add information for the contact regions. This feature is useful for special joints in structural analysis such as welds or rivets, or in thermal analysis if some sort of insulating film or barrier is used. However, if no special phenomenon is present, allowing the contact regions to be program controlled based on material properties previously assigned will suffice.

The next step was to mesh the model. Mesh quality was not entirely important in all places other than the coils, which are the most thermally involved components of the system. Mesh relevance describes the coarseness or fineness of the mesh, with -100 being the coarsest and 100 being the finest. For this case, a mesh with a relevance of 0 was used, with refinements added to decrease the mesh size on all faces of the coils added.

The next and most important steps of the model involve the heat generation and dissipation in the coils. The first step was to model the heat generated in the coils. The current input is a known value of 3 amps of load for failure, but for the purpose of the model and verification, the coil will be studied at 1 amp, 2 amps, and 3 amps. It must be determined how much heat is generated from these amounts of current. This heat comes from the resistive heating effect of copper as current passes through it. The equation for resistive, or Joule, heating relates power and two of the three of voltage, current, and resistance as follows [Incropera]. It is important to note that using Joule heating to calculate heat produced in the coils is a conservative estimate, as there will be mechanical and other electronic circuit heat losses in other parts of the system. However, these losses have been proven to be small, and Joule heating provides a good estimate for the heat produced [Staton 2005].

$$P = I^2 * R = V * I = \frac{V^2}{R}$$

For this application, the load current is known and will be varied. Therefore, determining the resistance of the wire per unit volume will allow for the calculation of

the power produced per unit volume in  $W/m^3$ , which is the required input to the FEA tool ANSYS. From the motor data sheet, the terminal resistance of the coil from phase to phase is 2.3 ohms. This can also be verified by using an ohmmeter to measure the resistance across one phase of the motor. The motor is a three phase motor, but only two phases are kept high at a time during normal operation. Therefore, the total resistance across the copper is 4.6 ohms at any given time. The power can then be calculated using the Joule heating equation given above. For the 3 amp case, the power is as follows:

$$P = I^2 * R = (3 A)^2 * 4.6 \Omega = 41.4 W$$

The volume of the coils that the 41.4 W is distributed across is given in the CAD tool to be  $1.67*10^4 \text{ mm}^3$ , or  $1.67*10^{-5} \text{ m}^3$ . Therefore, the value for internal heat generation across the coils is  $2.48*10^6 \text{ W/m}^3$  when 3 Amps are applied. Likewise, the same calculation was used for the 1 amp and 2 amp cases. The heat generation values for each of the loading conditions are summarized in the table below.

Load	Heat Generation ( $W/m^3$ )
1 A	$2.75*10^5$
2 A	$1.10*10^6$
3 A	$2.48*10^6$

Table 2: Heat Generation for Different Loading Conditions

The final step in determining the input information was to determine how the heat is transferred away from the coils in the form of convection and conduction. Conduction

is automatically accounted for in the contact surfaces using the prescribed thermal conductivity values. Convection, on the other hand, requires more work, and accurate modeling can be quite complicated. ANSYS simplifies the process by allowing the user to select surfaces and specify the heat transfer coefficient,  $h$ , and the ambient temperature. This is an approximation of a complicated phenomenon, but generally provides accurate enough results. Like radiation, rough estimates can be used to determine how much heat is transferred convectively relative to conductively. The equation for convection is shown below [Kays].

$$Q_{conv} = h * A * \Delta T$$

Therefore, the ratio of convective to conductive heat transfer simplifies to the ratio of  $h$  to  $\kappa$ , or the ratio of the convective heat transfer coefficient to the thermal conductivity.

Convection can be simplified into two different forms. Natural convection occurs between a body and a fluid when the fluid does not have a velocity imposed on it, and forced convection occurs when the fluid is forced to move past the body. Forced convection has much higher heat transfer coefficients, but requires some sort of mechanism to move the fluid. In the case of the flat motor, the rotor rotates at very high speeds, suggesting excellent forced convection. However, as mentioned above, the motor will be studied in an isolated motionless state to simplify the modeling and verification, while still providing an adequate model for the determination of heat sink improvements. Therefore, for this case, natural convection will be applied to all exposed surfaces of the

motor. Tables can be found giving heat transfer coefficient approximations for different scenarios. For the purpose of this study, the natural convection heat transfer coefficient will be  $10 \text{ W/m}^2\text{K}$ . Therefore, for areas of high thermal conductivity such as the copper and aluminum, convection will account for less than 10 percent of the total heat transfer. However, for areas low thermal conductivity, such as the circuit board, convection should account for more heat transfer than conduction.

After inputting the internal heat generation and convection data, the model was ready for solving. The required solution information was specified as the temperature of the entire model. More detailed results will be presented later, as the results are examined more closely.

### *3.2 Results*

After solving the model for each of the three current loads, the next step was to understand the results. The temperature profile of the entire model was considered first. One of the advantages of ANSYS is that it gives the user the ability to study the temperature profile across the entire model, rather than at just one point, as a thermocouple would do. Therefore, the user gets a very comprehensive understanding of the temperature and heat flux of the model. The temperature profile of the motor for the 1 Amp case is shown below. All temperatures are shown in degrees Celsius, and the maximum temperature is  $36.4 \text{ }^\circ\text{C}$ .



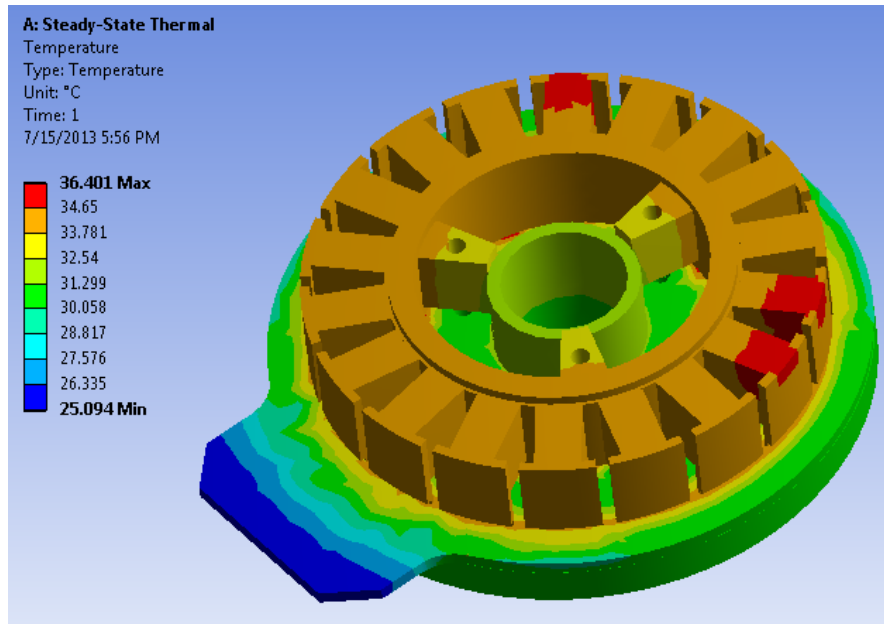


Figure 19: Temperature Profile of Motor (1 Amp Condition)

From the model, one can tell that the coils of the stator are the hottest part of the motor, which was expected as the coils are where the heat is generated. The visible temperature gradient, particularly in the circuit board, suggests different temperatures on the two sides of the board. This is due to the low thermal conductivity of the circuit board material, which traps heat on the coil side of the board, not allowing it to escape to the aluminum base beneath. It is interesting to note the temperature differences between the different coils. This appears to be largely due to the contacts between the coil housing and the part of the aluminum base that houses the shaft. The thermal conductivity of this path is very high, much higher than the circuit board or the convective heat transfer. This would provide a great heat sink path for the coils, but the contact area seems to be too small. The temperature of the coils close to this path is lowered, explaining the difference in coil temperatures.

As mentioned before, the coils are the part we are most concerned with, as they produce the heat and are subject to failure if the temperature gets too high. To further study the temperature profile of the coils, the set of data for the 1, 2, and 3 Amp conditions were isolated and shown below, to allow for more contrast in the color gradient. Even though the color scale makes the coils look like they have very different temperatures, the coolest coil was actually only about 0.5, 3, and 7 °C less than the hottest coil for the 1, 2, and 3 Amp cases respectively.

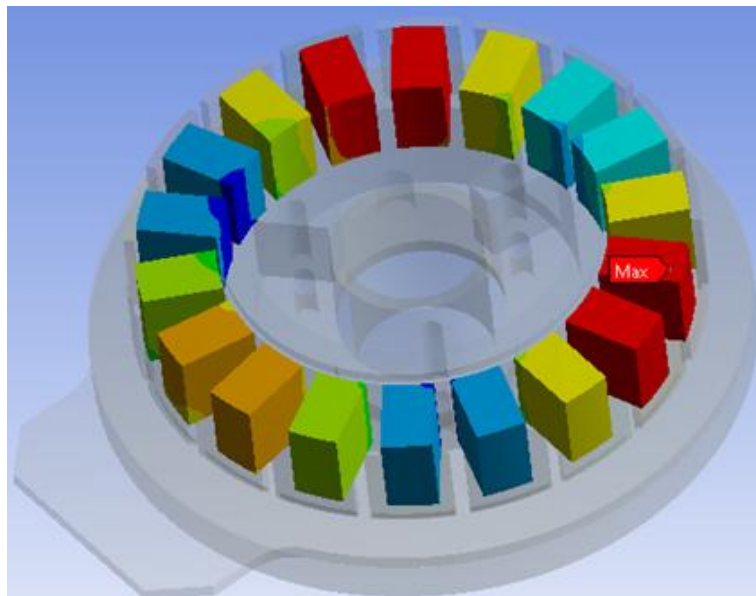


Figure 20: Temperature Profile of Coils with Point of Maximum Temperature Noted

Again, it is evident that the coils have different temperatures, explained by the contacts to the aluminum. On a more quantitative note, the maximum temperature of the coils for each of the load conditions is the important result, and is the value that needs to be lowered. The steady state value of the maximum temperature of the coils for each of

the 1, 2, and 3 Amp cases is shown below, along with a temperature profile of the entire motor.

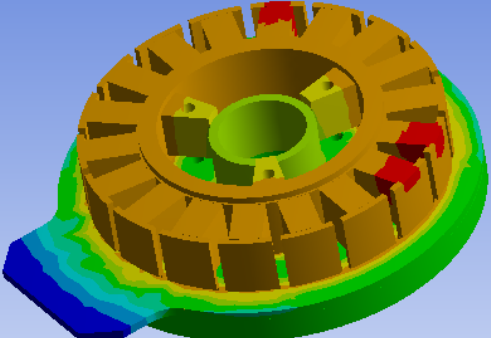
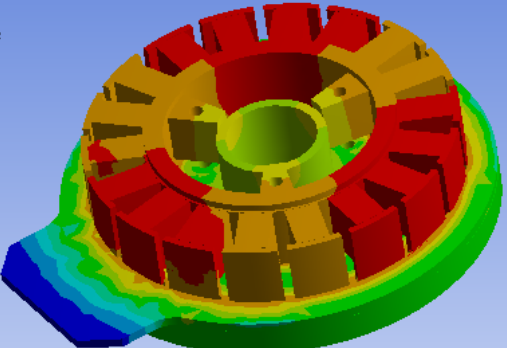
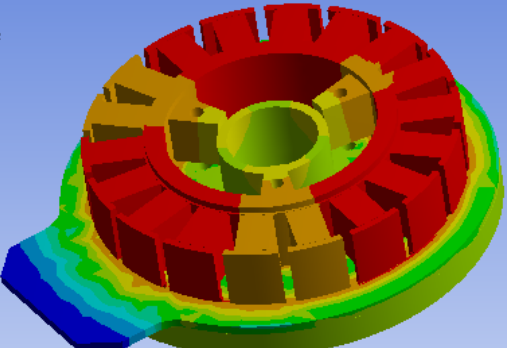
Load (A)	Maximum Coil Temperature (°C)	Temperature Profile
1	34.7	<p><b>A: Steady-State Thermal</b>            Temperature            Type: Temperature            Unit: °C            Time: 1            7/15/2013 5:56 PM</p>  <p>36.401 Max            34.65            33.781            32.54            31.299            30.058            28.817            27.576            26.335            25.094 Min</p>
2	72.6	<p><b>A: Steady-State Thermal</b>            Temperature            Type: Temperature            Unit: °C            Time: 1            7/15/2013 5:31 PM</p>  <p>79.536 Max            71.924            67.236            62.549            57.862            53.174            48.487            43.8            39.112            34.425 Min</p>
3	136.0	<p><b>A: Steady-State Thermal</b>            Temperature            Type: Temperature            Unit: °C            Time: 1            7/15/2013 5:17 PM</p>  <p>151.44 Max            133.07            122.71            112.34            101.97            91.604            81.236            70.868            60.501            50.133 Min</p>

Table 3: Maximum Coil Temperature at Various Loads

As mentioned earlier, the coil failure temperature is 125 °C. The model predicts that the steady state temperature at 3 Amps would be 136 °C, implying that the coils will fail under the 3 Amp condition. This has been backed up by observations of this motor running at 3 Amps in the past, but will also be tested experimentally to validate the FEA model. An image showing an example of severe coil failure in an overheated motor is shown below.



Figure 21: Coil Failure on Old Motor Due to Overheating

It must be noted that the model presented thus far is a simplified scenario of the actual motor conditions. In operation, this motor would have a rotor forcing convection

above the coils and heat sink grease on the base. The duty cycle is also different for this simplified case. Normal operation would require each phase of the motor to run at 3 Amps and provide 48 Volts with a duty cycle of around 60 percent. However, to simplify the experimentation, the model was simulated with only two phases running at 100 percent duty cycle providing 3 Amps. These conditions provide a good estimate of the actual conditions and allow for more repeatable testing with a simple power source. The next steps will be to validate this model using experiments on the actual motor and then move forward with the modifications and optimization.

#### 4. Validating the Model

After establishing a finite element model, the results had to be validated using experiments on the actual model. Two components were required for the experimental set up, a power source and a temperature sensor.

A power source capable of supplying variable current amounts up to 6 Amps was used. As mentioned, the motor will only ever have two poles at high with a 100 percent duty cycle, with the other at low. The power supply was used to supply 1, 2, or 3 Amps of current to phases 1 and 2 through pins 7 and 8 for consistency, while pin 6 was held at ground. Before the testing was started, the resistance across each pole was checked to ensure it was within 0.1 ohms of the expected 2.3 ohms. A pin out for the motor can be found in Appendix D.

Temperature sensing is generally done using thermocouples or thermistors. These options, although fairly reliable, are limited in that they may only be placed at one location. Another option available was an infrared thermometer, which determines the

temperature of any black body that the laser is shined upon. This option is very easy to use and allows multiple measurements to be taken across different points of the motor coils with good accuracy. This method of sensing was used for the experimental validation. Although there is no automated data capture with a temperature gun, temperature measurements from the gun were manually recorded every 20 seconds to capture the data and provide a record of the temperature change over time. The experimental setup is shown below.

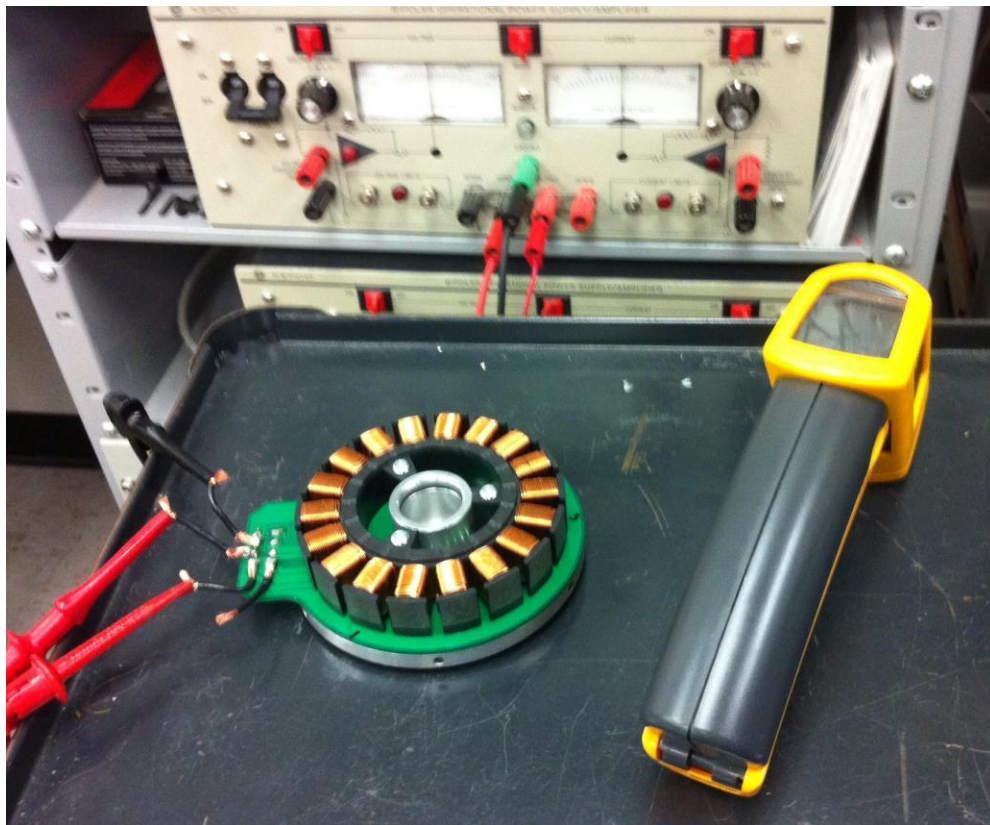


Figure 22: Experimental Setup

Each test was started by turning on the power supply to a room temperature motor (coil temperatures between 22 and 25 °C) and using the gun to measure the maximum temperature on a coil every 20 seconds. Data collection was ended when the maximum temperature stayed constant for 2 minutes, signifying steady state. This was done for the 1, 2, and 3 Amp conditions, with measurements taken for four different coils for each of the load conditions, to provide a total of 12 data sets. An average of the four trials was calculated for each of the amp conditions by averaging the results. Examples of this averaging technique are shown below for the 1, 2, and 3 Amp case. The average steady state coil temperatures are 34.4 °C, 68.1 °C, and 133.8 °C respectively.

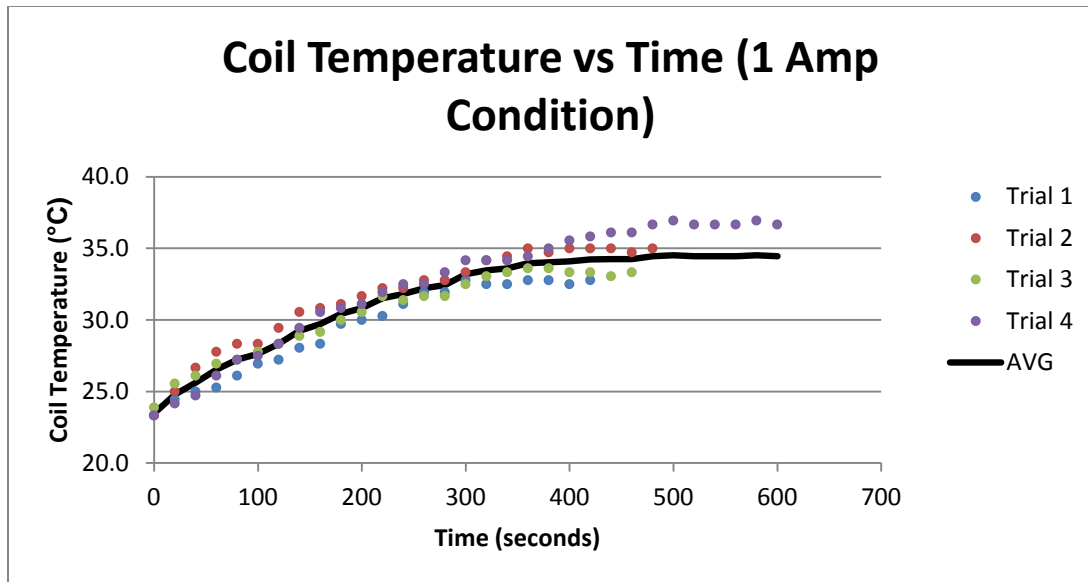


Table 4: Averaged 1 Amp Coil Temperature over Time (34.4 °C Steady State)

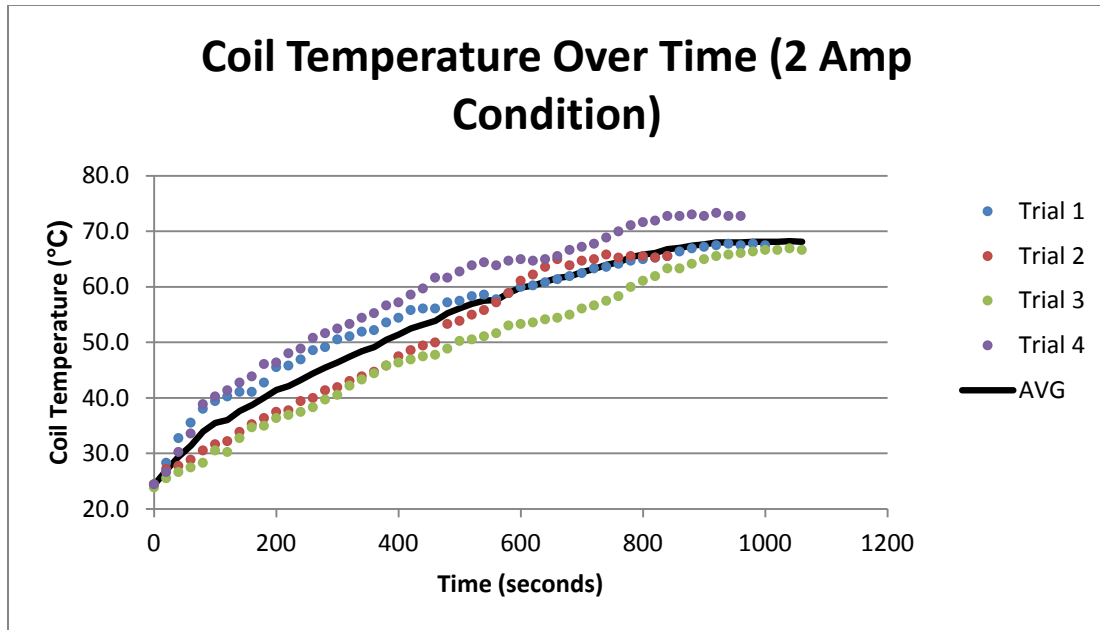


Table 5: Averaged 2 Amp Coil Temperature over Time (68.1 °C Steady State)

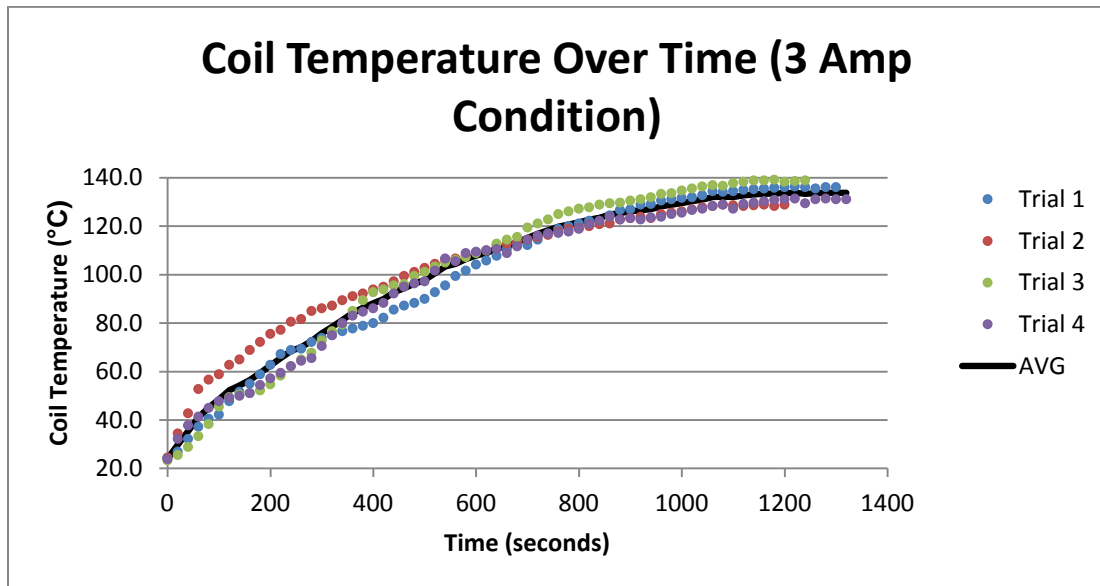


Table 6: Averaged 3 Amp Coil Temperature over Time (133.8 °C Steady State)

The averaged results of these experiments are shown below for the 1, 2, and 3 Amp case.



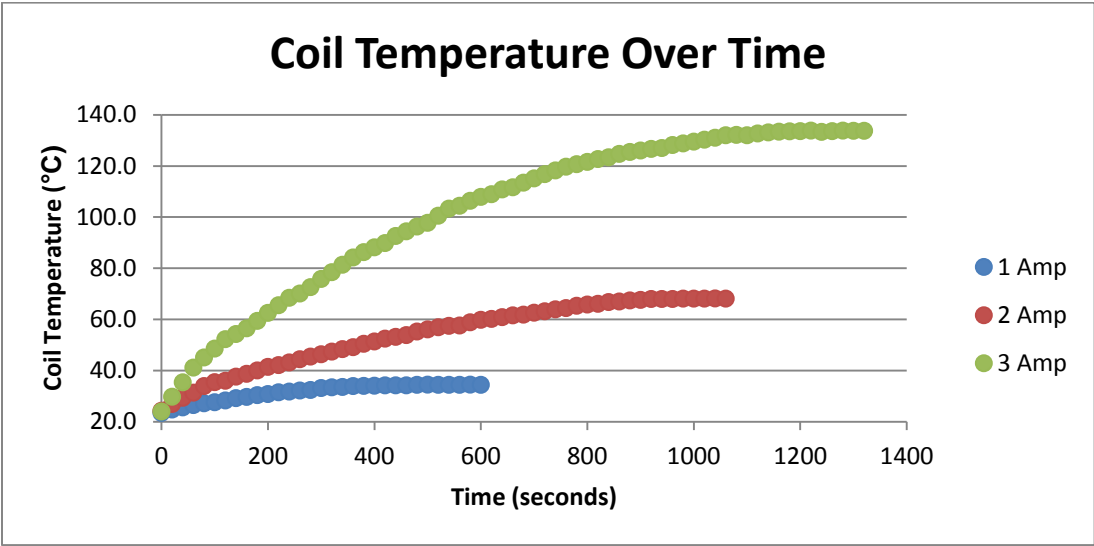


Figure 23: Coil Temperature as a Function of Time for Various Applied Currents

From the results, the steady state maximum coil temperature can be determined for the 1, 2, and 3 Amp cases to be 34.4 °C, 68.1 °C, and 133.8 °C respectively. A table summarizing the physical results and comparing them to the FEA predicted results is shown below.

	1 Amp	2 Amp	3 Amp
<b>FEA (°C)</b>	34.7	72.6	136.0
<b>Experimental (°C)</b>	34.4	68.1	133.8
<b>Percent Error</b>	2.6	9.1	1.9

Table 7: Comparing ANSYS and Experimental Results

From the table, the FEA results match the experimental results very well, to within 5 degrees Celsius for each load condition. The percent error was calculated by

dividing the difference in FEA and experimental results by the total temperature increase for each case and multiplying by 100, giving the final temperature difference as a percent of the total increase during the trial. Percent error was low for all conditions, staying at less than 10 percent for the 2 Amp condition and close to 2 percent for the 1 and 3 Amp conditions. Importantly, the experimental results were all slightly lower than the FEA predicted values. This consistency implies that the model correctly predicted the thermodynamic behavior of the actual motor, confirming the assumed convection heat transfer coefficient and resistive heat generation.

Another interesting take away from the experimental validation was related to coil failure. As mentioned, the coils are rated to fail at 125 °C. From the results, the maximum coil temperature reached was around 134 °C. This implies that failure should have occurred. Upon close inspection, it was evident that small bubbles began to form on some of the coils in places where the coating of the copper wire began to peel back from the wire, as shown below. Because the temperature did not vastly exceed 125 °C, the damage was minimal, and the motor was still operational. However, operation under these conditions for too long will lead to greater failure, as referenced previously, and should be avoided.

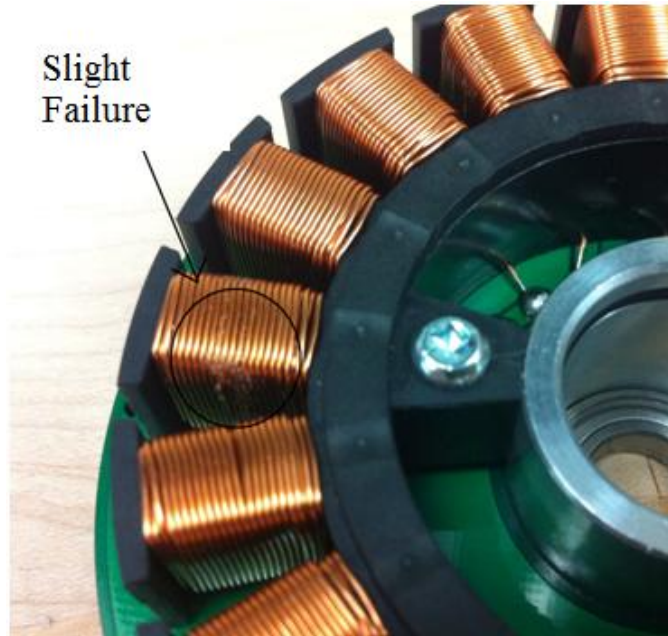


Figure 24: Image Showing Minor Coil Failure from 3 Amp Load

#### 5. Redesign Solution and Optimization

Once a model for the flat motor had been established and verified, a redesign was attempted. In looking at the model, the heat flow, and the parts of the motor that are capable of being altered, a solution needed to be reached to transfer more heat away from the coils so that the maximum coil temperature is lowered.

The point of maximum temperature on the coils occurred towards the lower part of the coil, where the heat is transferred from the coils to the circuit board through a small cross sectional area of conduction and convection heat transfer with stagnant air. The circuit board, which has a low thermal conductivity, traps much of the heat, not allowing it to escape to the highly conductive metal below. Since the electronics of the motor and circuit board are simple, there is much room to add paths for heat transfer through the board. One such solution would be to replace part of the circuit board with a more

thermally conductive material that is still an electrical insulator to prevent tampering with the electronics of the board. One such option is a material known as Gap Pad, made by The Bergquist Company in Chanhassen, MN [Berqguist]. Gap Pad has good thermal characteristics while maintaining electrically insulating properties [Appendix E].

Another option that the FEA results point to would be to increase the contact area between the coil housing and the inner aluminum base. From the FEA results, the maximum heat flux into the inner base is greater than  $95,000 \text{ W/m}^2$ , shown in the figure below, compared to less than  $7,900 \text{ W/m}^2$  maximum through the circuit board, suggesting much less heat through a much greater area. Additionally, the  $95 \text{ kW/m}^2$  to the base occurs where the existing contacts are located, compared to less than  $15 \text{ kW/m}^2$  at areas with no contact to the coil housing. These results point to adding additional “contacts” in the large gaps between the coils and the inner base to increase the heat transferred away from the coils. This option will be examined using the FEA tool and compared to the Gap Pad option.

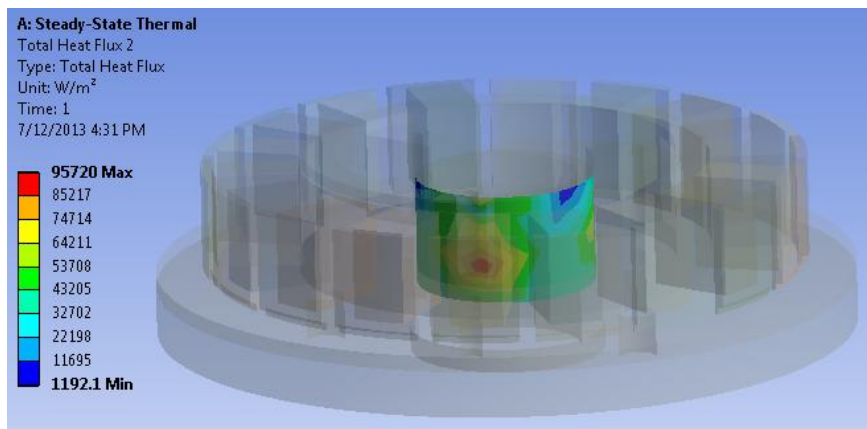


Figure 25: Inner Base Total Heat Flux

First, replacing the circuit board with Gap Pad will be considered. The design challenge was to determine how much of the Gap Pad to use, a design task that an FEA tool can help with. Cutting into a circuit board is not reversible, so physical experimentation should be done carefully after FEA consultation first. Using the validated finite element model, an optimization routine can be run to determine the most effective location and amount of Gap Pad to use to lower the temperature of the coils. An initial tool to help in the placement of the Gap Pad was the heat flux data through the circuit board from the previous ANSYS study. The heat flux data is shown below. As expected, most of the heat travels through the board at the area under the coils, suggesting a “ring” shaped Gap Pad insert may be helpful in improving the heat transferred at that area.

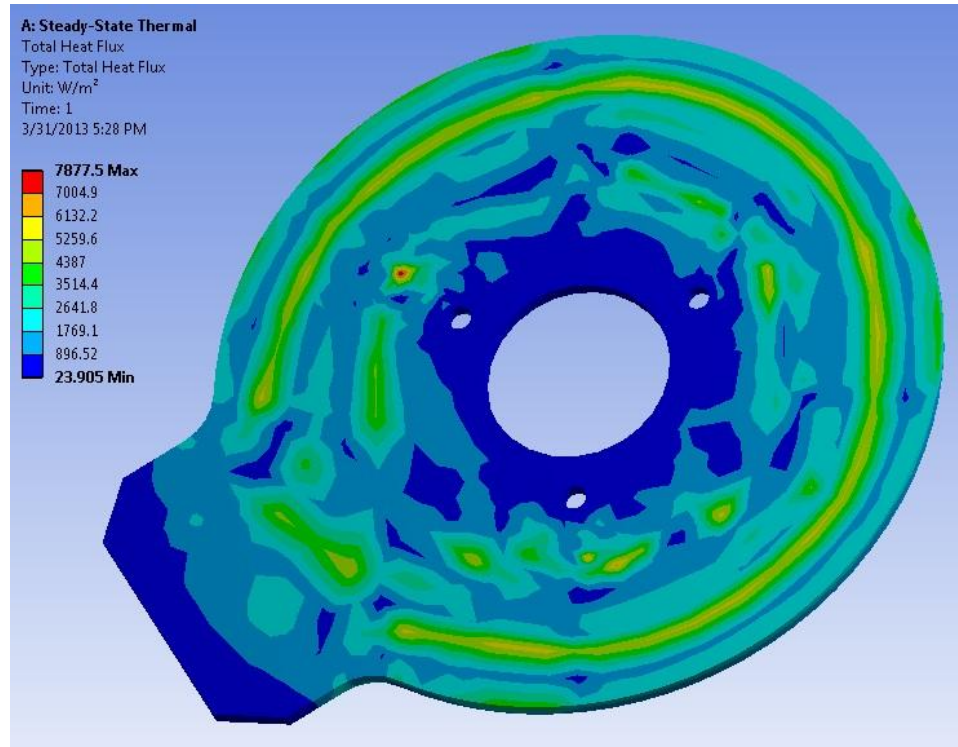


Figure 26: Circuit Board Total Heat Flux

The first step in the FEA optimization process was to actually change the geometry to add the Gap Pad so that it could be optimized. This was done in the DesignModeler module. The Gap Pad ring was sketched and added to the model. In order to best optimize the Gap Pad, both the width of the pad and the inner diameter of the ring were selected as parameters for optimization. These will both be varied to determine the effect they have on the coil temperature. The resulting geometry, with the Gap Pad insert in place, shown here with an inner diameter of 65 mm and a width of 5 mm, is shown below.

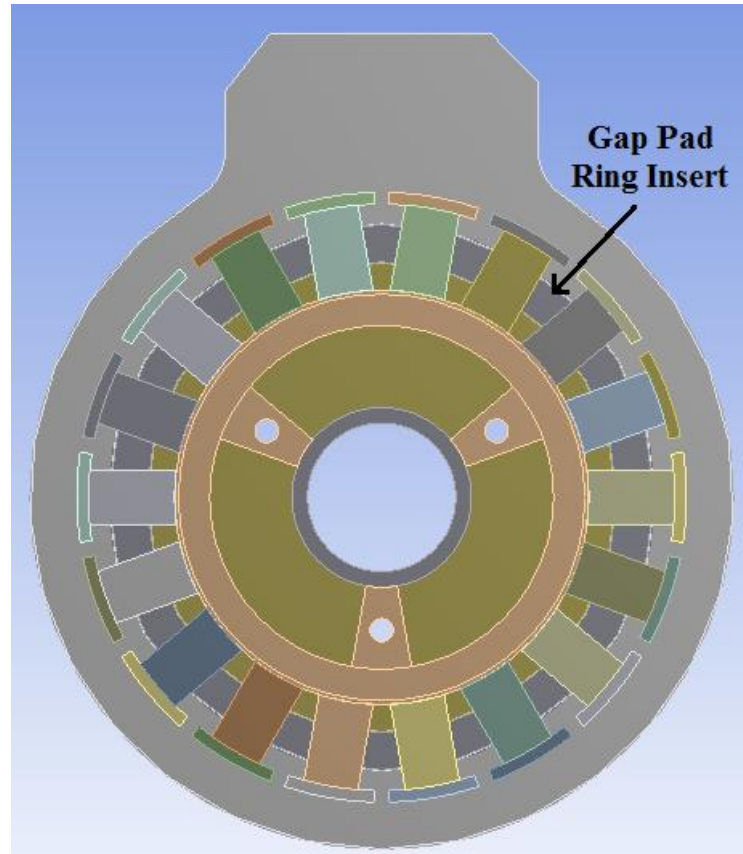


Figure 27: Top View of Motor with Gap Pad Insert

The next step was to ensure that all of the external conditions from the first model were still in place. Identical conditions must be used in the optimization to ensure the validity of the study. This was easily done as FEA tools preserve all of the model data even when changes to the geometry are made. The only change that had to be made was adding the material properties for the Gap Pad ring. For this study, Gap Pad 1500 was selected, as it provides a thermal conductivity of  $1.5 \text{ W/m}^2\text{K}$ , much higher than the  $0.27 \text{ W/m}^2\text{K}$  of the circuit board [Appendix E]. For the purposes of the optimization, the 3 Amp case was used. The same solution can still be applied to the other load cases with similar results.

Just as the width and diameter of the Gap Pad ring were specified in DesignModeler as parameters which will be varied, the parameter that will be optimized, the maximum coil temperature in this case, must also be specified. Since all of the model information should still be in place, the next step was to begin the optimization by adding the “Goal Driven Optimization” module to the model. Opening the “Design of Experiments” section allows the user to specify a range and distribution of data points for which it will solve the problem. In this case, the Gap Pad width will range from 0.5 mm to 10 mm, and the inner diameter of the ring will range from 60 mm to 72 mm. The data points to test were then auto generated using an optimal space-filling design algorithm. The tool then solves the model using each of these design points, and returns the maximum coil temperature, as requested. The 10 data points and the corresponding maximum coil temperature are shown below.

Gap Pad Width (mm)	Inner Diameter of Ring (mm)	Maximum Coil Temperature (C)
0.56	66.0	106.9
1.67	60.7	105.9
3.89	63.3	105.6
2.78	68.7	103.8
7.22	62.0	101.3
5.00	71.3	100.6
6.11	67.3	99.8
9.44	64.7	99.1
8.33	70.0	99.1

Table 8: Gap Pad Width and Diameter Design Points with Resulting Coil Temperature



From this data, a “Response Surface” was generated to better visualize the data by showing the maximum coil temperature as a function of both the Gap Pad width and diameter. This response surface is shown below from two different vantage points, with both the surface of best fit, as well as the actual data points.

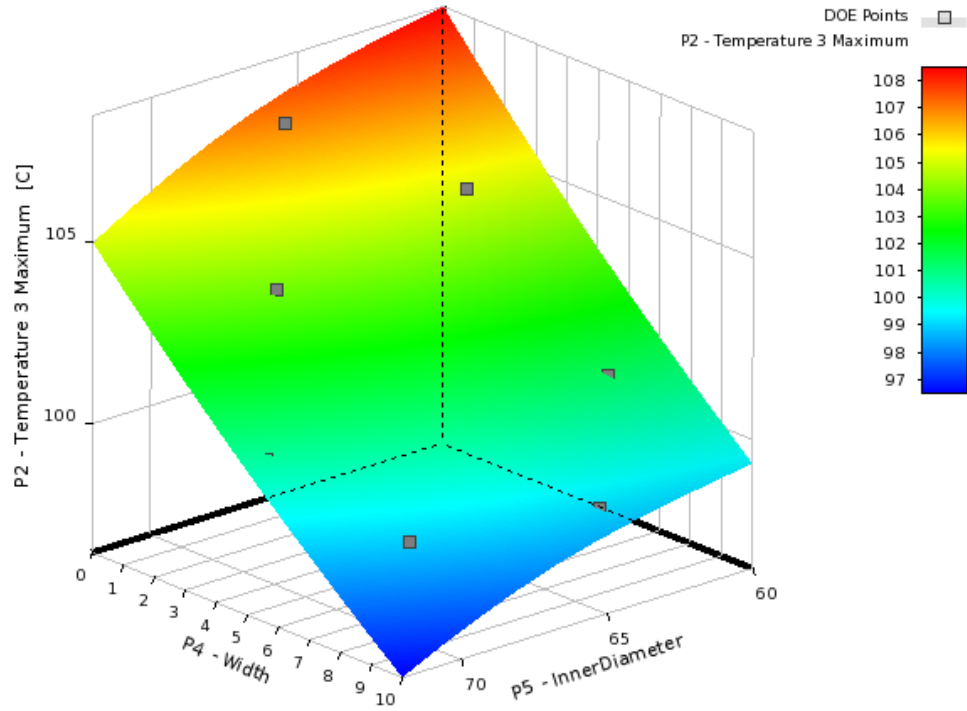


Figure 28: Maximum Temperature as a Function of Width and Diameter of Gap Pad (View 1)

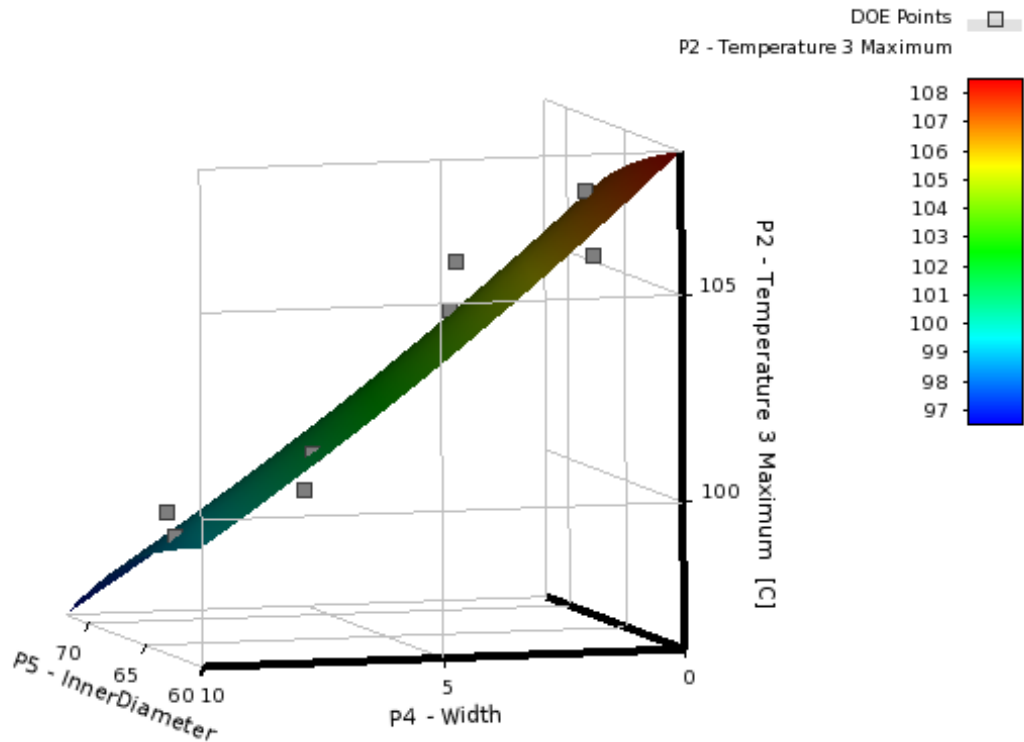


Figure 29: Maximum Temperature as a Function of Width and Diameter of Gap Pad (View 2)

From the graph, it can be gathered that in general, points with high coil temperatures had small diameters and small widths, and points with low coil temperatures had large diameters and large widths, corresponding to large surface areas of Gap Pad. This suggests that the Gap Pad must be located as far away from the center of the motor as possible, with as wide of a ring as possible. This study also suggests that adding a Gap Pad ring to the motor will decrease the steady state temperature from 134 °C to less than 105 °C for the 3 Amp condition.

As mentioned, another option to help heat sink the motor in addition to the Gap Pad ring addition is to increase heat flow to the inner aluminum base by improving its contact with the coils. To do this, it was proposed to add aluminum contacts to provide a

conductive path for the heat to flow. Aluminum was chosen as a material, rather than Gap Pad, due to its higher thermal conductivity and because the location of the contacts does not require electrical insulation. The proposed modification is shown in CAD form below.

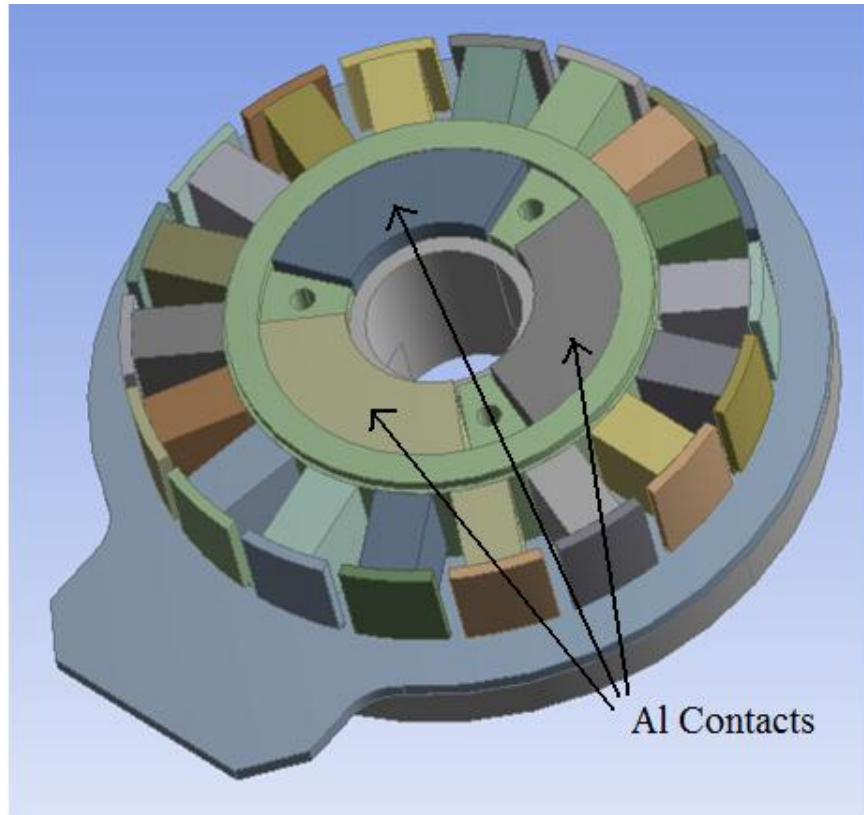


Figure 30: CAD Model of Motor with Aluminum Contacts

This new CAD model with contact modifications was simulated using the FEA study with the same conditions which had previously been validated. The results of the study are shown below.

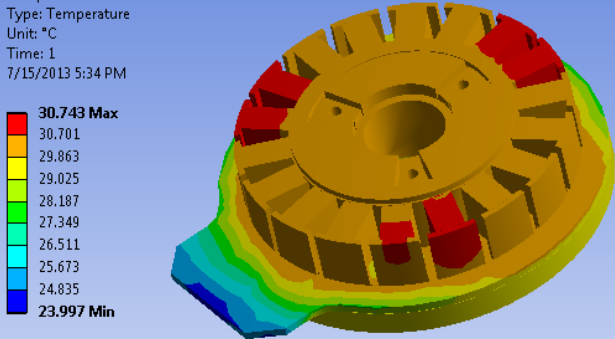
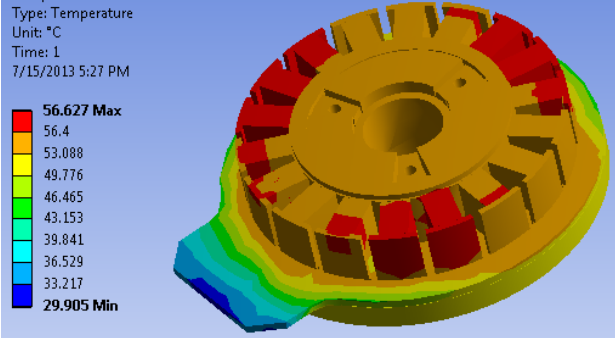
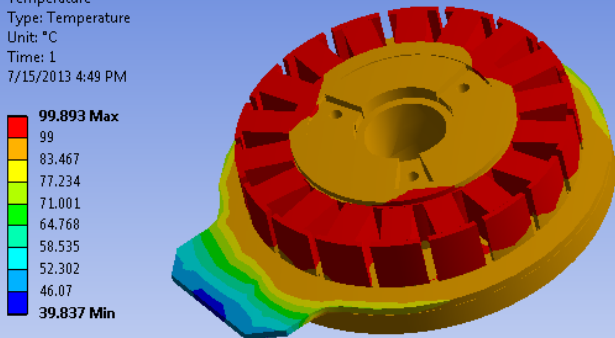
Load (A)	Maximum Coil Temperature (°C)	Temperature Profile
1	30.7	<p><b>A: Steady-State Thermal</b>            Temperature            Type: Temperature            Unit: °C            Time: 1            7/15/2013 5:34 PM</p> 
2	56.6	<p><b>A: Steady-State Thermal</b>            Temperature            Type: Temperature            Unit: °C            Time: 1            7/15/2013 5:27 PM</p> 
3	99.8	<p><b>A: Steady-State Thermal</b>            Temperature            Type: Temperature            Unit: °C            Time: 1            7/15/2013 4:49 PM</p> 

Table 9: Motor with Aluminum Contacts Maximum Coil Temperature at Various Loads

Similar to the Gap Pad modification, the FEA results predict that the aluminum contacts should also significantly lower the maximum coil temperature by increasing the amount of heat transferred to the aluminum base.

One final FEA test was performed to determine how the motor would react with both the Gap Pad and the aluminum contacts. The CAD model is shown below.

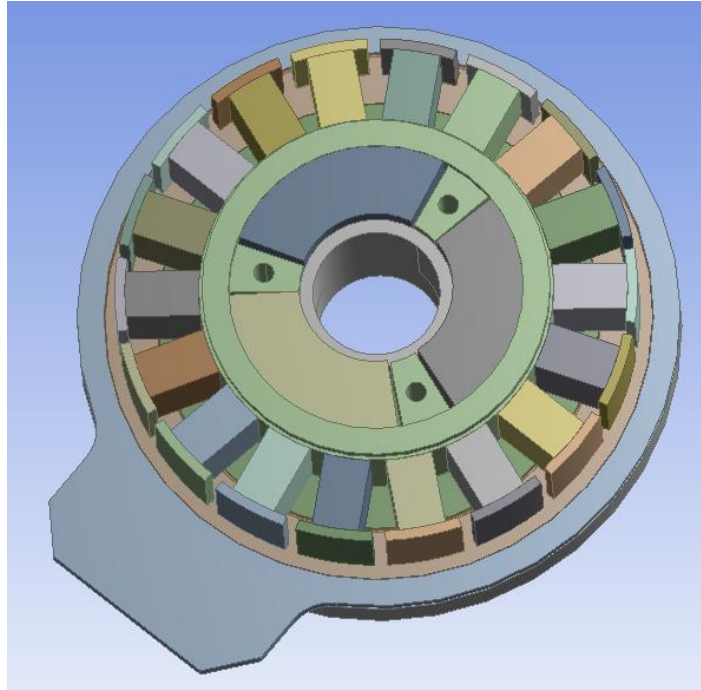


Figure 31: CAD Model of Motor with Gap Pad and Aluminum Contacts

Again, the new model was analyzed using an identical FEA model, and the resulting maximum coil temperature and temperature profile are shown below.

Load (A)	Maximum Coil Temperature (°C)	Temperature Profile
1	30.2	<p>A: Steady-State Thermal Temperature Type: Temperature Unit: °C Time: 1 7/15/2013 6:54 PM</p> <p>30.618 Max 30.134 29.632 28.851 28.069 27.288 26.506 25.725 24.943 24.161 Min</p>
2	55.2	<p>A: Steady-State Thermal Temperature Type: Temperature Unit: °C Time: 1 7/15/2013 6:47 PM</p> <p>56.954 Max 54.831 52.312 49.242 46.171 43.101 40.031 36.96 33.89 30.819 Min</p>
3	96.8	<p>A: Steady-State Thermal Temperature Type: Temperature Unit: °C Time: 1 7/15/2013 6:43 PM</p> <p>100.82 Max 95.672 88.96 82.248 75.536 68.824 62.112 55.4 48.688 41.976 Min</p>

Table 10: Motor With Gap Pad and Aluminum Contacts Maximum Coil Temperature

These results are slightly better than both the Gap Pad and the aluminum contacts by themselves, but only by a small amount, suggesting that the benefit of adding both modifications is not cumulative. However, this model did perform the best, and if the FEA model is correct, which the validations have proven, then adding the Gap Pad and aluminum contacts should lower the steady state temperature by around 35 degrees Celsius. The next step will be to implement these modifications and test the optimized motor.

## 6. Optimized Prototype

After an optimized solution was reached, the next step was to test this solution by making the modifications to the model and testing the resulting prototype. This is an important step in the redesign process, as it confirms that the redesign was actually successful and helps to demonstrate the new model. Since the original model has already been verified, the redesign should be successful, and the results should have lower maximum coil temperatures than the original motor.

The first step in making the prototype was to take the motor apart. The coils were unscrewed and the solder was removed so the circuit board could be lifted off the aluminum base. The resulting circuit board is shown below.

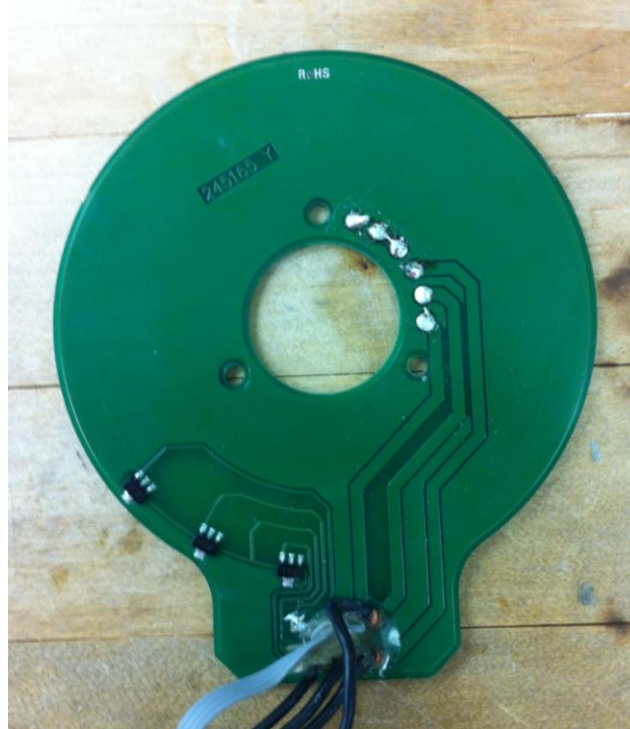


Figure 32: Motor Circuit Board

From the figure, the electric current paths, which carry current to the coils, can be seen on the right. Wiring for the Hall Sensors on the left should also be noticed. These pathways represent areas that, if cut into, require rerouting of the wiring. A 10 mm ring at 68 mm in diameter (the highest possible while still remaining on the circuit board) was sketched onto the circuit board and cut out. The Gap Pad, which is very compliant and slightly tacky, was then inserted into the cut out section, making sure that the fit was snug to ensure good contact regions at the circuit board and base to maximize the heat transfer. The resulting system is shown below.



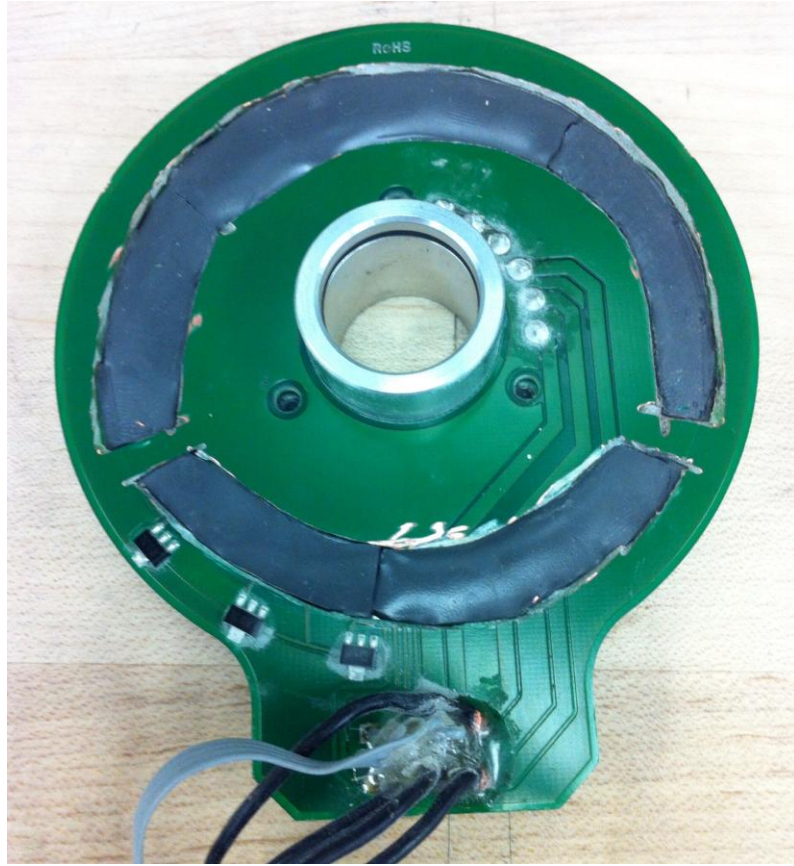


Figure 33: Motor Circuit Board with Gap Pad Insert

After the Gap Pad had been inserted, the next step was to rewire the motor to account for the severed paths in the circuit board. Wires were soldered onto the leads at the center of the coils to allow for connection to the power source. The resulting motor is shown below, with the ground wire and three wires for the three phases of the motor noted.

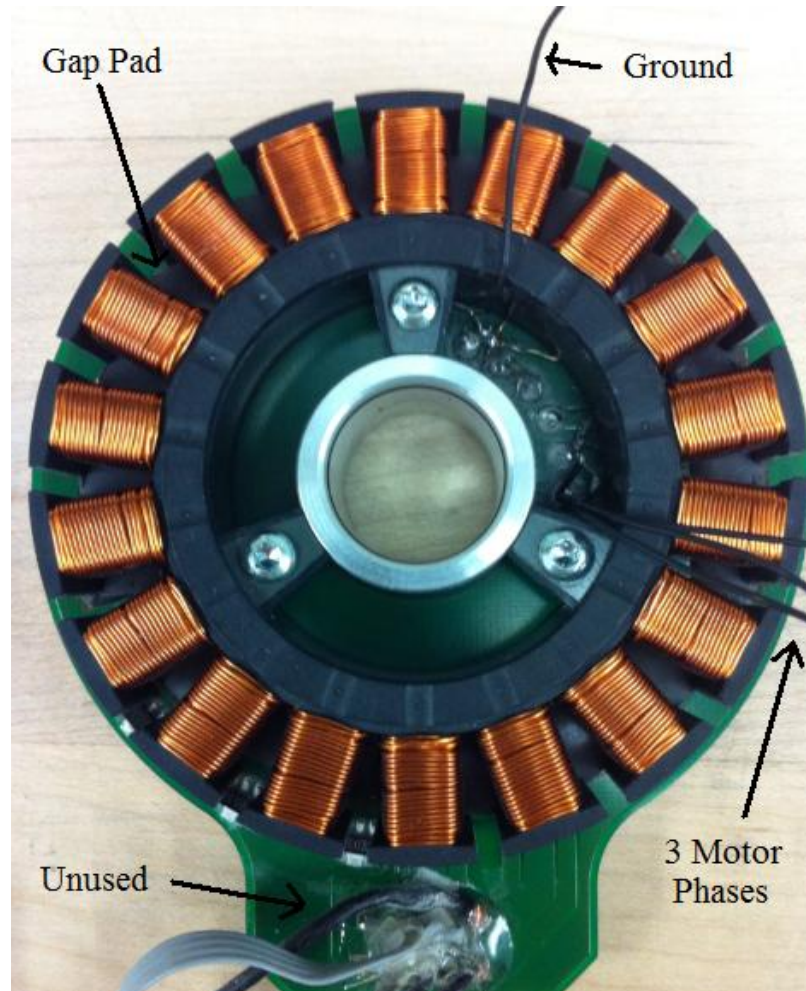


Figure 34: Motor with Gap Pad and Rerouted Wiring

The next step was to make the modified aluminum contacts motor. A piece of aluminum was machined into three pieces to fit the three spaces in the motor, making sure the fit was tight to ensure good contact for the conduction paths. The modified motor is shown below.

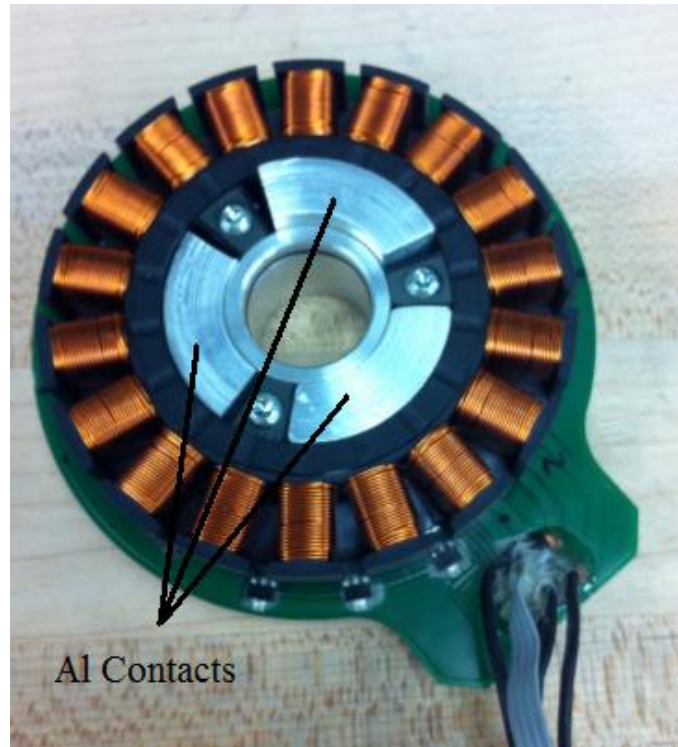


Figure 35: Motor with Aluminum Contacts

Finally, the motor with the Gap Pad and aluminum contacts was constructed. This was done by simply inserting the aluminum contacts into the motor with the Gap Pad already installed. Thermal grease was considered as an option for improving contact. However, the well machined contacts make sufficient contact with the motor, and thermal grease does not provide any advantage outside of increased contact area. The completed motor is shown below.

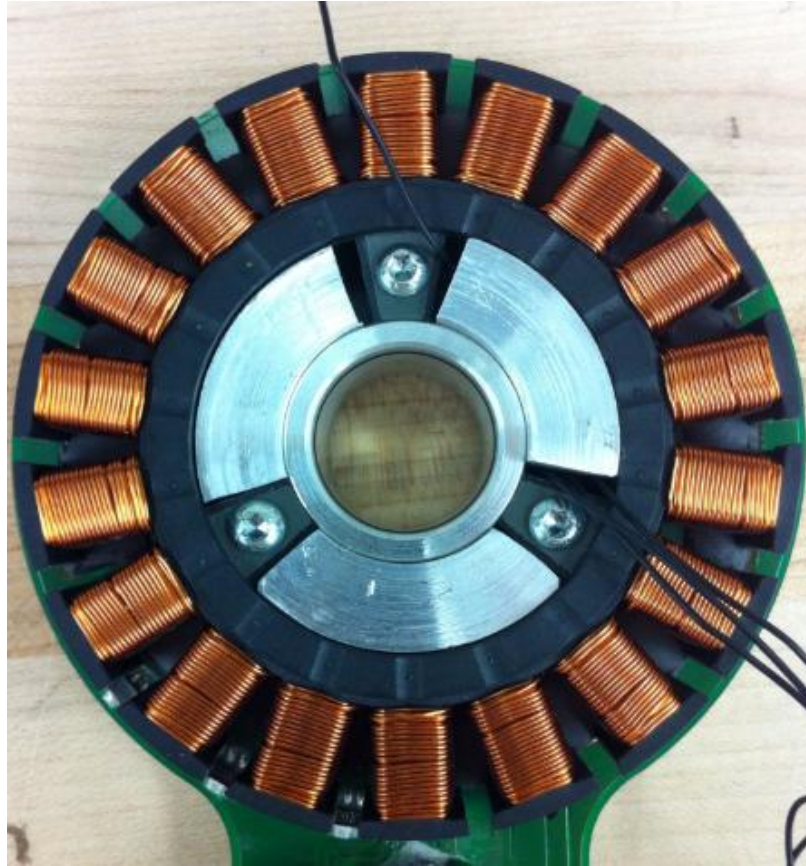


Figure 36: Motor with Gap Pad and Aluminum Contacts

Testing of the three prototypes was done in the same manner as the verification process, using a power supply and infrared thermometer to take temperature readings at the hottest point on 4 different coils every 20 seconds until steady state was reached. The results are shown below, in graphical form first, with a separate graph for each of the load conditions, each showing the results of the motor as built, with the Gap Pad, with the aluminum contacts, and with both the Gap Pad and contacts for comparison.

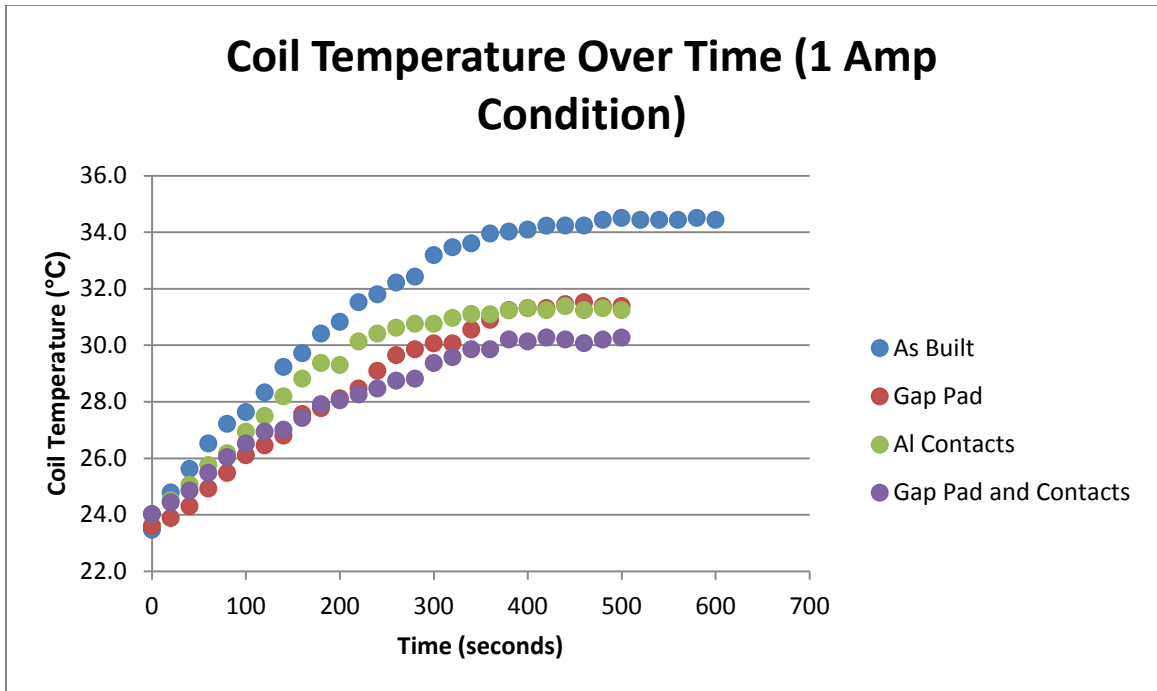


Figure 37: 1 Amp Maximum Coil Temperature Comparison

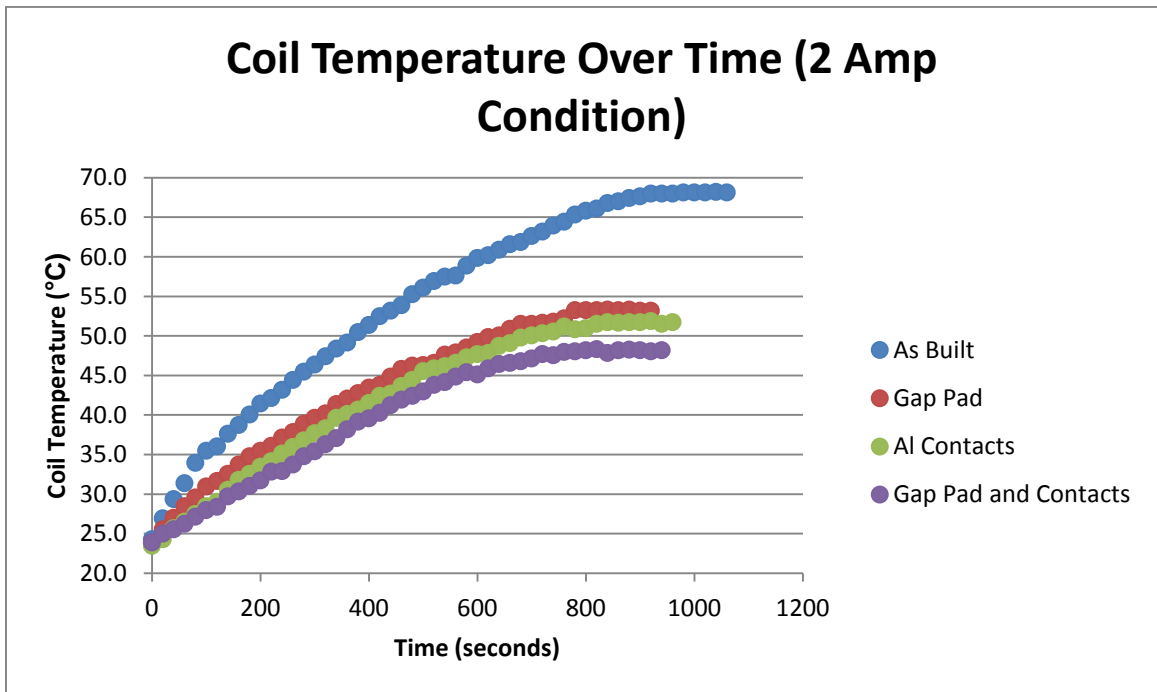


Figure 38: 2 Amp Maximum Coil Temperature Comparison

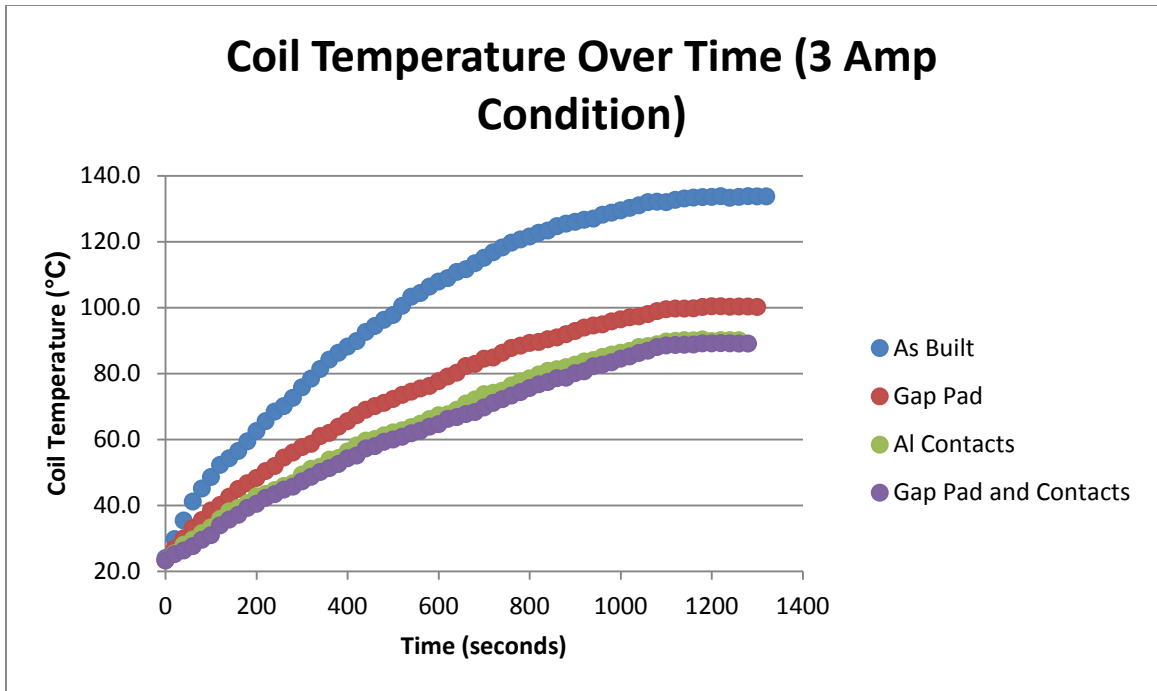


Figure 39: 3 Amp Maximum Coil Temperature Comparison

A table summarizing the maximum steady state temperature for each load condition from the original motor and the all three of the modified motors, as well as the percent difference for each modification is shown below.

	1 Amp	2 Amp	3 Amp	AVG
As Built	34.4	68.1	133.8	
Gap Pad	31.4	53.3	100.2	
% Difference	26%	33%	30%	30%
Al Contacts	31.3	51.7	90.2	
% Difference	27%	36%	39%	34%
Gap Pad and Contacts	30.3	48.2	89.1	
% Difference	36%	44%	40%	40%

Table 11: Comparison of Maximum Coil Temperatures (°C)

From the results, it is clear that all three of the modified motors provided noticeably lower maximum coil temperatures. The aluminum contacts performed slightly better than the Gap Pad, and the combination of the two slightly better than that.

## 7. Conclusions

First, when looking at the literal results of this study, it is evident that a flat motor was successfully thermally modeled operating at steady state conditions with loads of 1, 2, and 3 Amps. This model was then verified experimentally to validate the choice of material properties and convection coefficient in the finite element analysis program. Next, it can be assumed that embedding Gap Pad material in the circuit board of the motor effectively lowers the steady state temperature of the coils by around 30 percent of the total temperature increase. Similarly, it was shown that adding thermally conductive pieces to increase contact between the coils and the inner aluminum base lowers the coil temperatures by around 35 percent. Finally, the combination of these two modifications lowers the coil temperature by around 40 percent of the total temperature increase. Further analysis could be run to determine at what current the motor could be run before failure is reached, determining the exact increase in operating conditions. The coil temperature decrease can certainly be enough to prevent the motor from overheating in certain operating conditions under which the motor may otherwise fail, suggesting the heat sinking modifications were successful.

Other than the heat sinking modifications, this chapter also focused on using FEA as an aid in the redesign process. The FEA tool was successfully used to provide reasonable approximations of the thermal characteristics of the motor, both as built and

with the modifications. Through the FEA studies, the modifications were tweaked and optimized quickly, efficiently, and cost effectively.

One benefit of the studies performed was the simplified nature of analysis. Rather than studying a flat motor in full normal operation in a prosthetic, the system was isolated and simplified to allow for ease of testing and fewer assumptions. The results can then be scaled up and applied to the actual motor.

Another noteworthy part of this study was the complexity of modeling convection. Convection is an extremely complicated phenomenon in nature. In these studies, a simplified form of convection modeling was used requiring only a convective heat transfer coefficient and surroundings temperature. While this may slightly limit the accuracy of the results, the experimental verification helped to validate the model. Additionally, another beneficial aspect of the optimization study is that it is more focused on the relative results of changing a parameter, rather than the absolute values. Therefore, if the FEA predicted values are slightly off, the optimization values will be off in the same direction, leading to correctly predicted relative increases from the optimization. For these studies, the FEA predicted temperatures were on average slightly higher than the experimental values for both the as built motor and the motors with modifications. This small error could be contributed to the fact that it is difficult to find the true maximum using the temperature sensor gun, whereas the FEA study can determine the temperature at every point on the coils. It could also be contributed to the fact that radiation was neglected, giving slightly higher results for the FEA study compared to the experimental model in which radiation was a small factor. Regardless, this error is acceptable because it was consistent, meaning that the relative improvement from the



modifications was correctly predicted and optimized. A summary chart of the error is shown below. In general, the ANSYS results were slightly higher than the experimental results, particularly for the 2 and 3 Amp cases, which is acceptable due to the consistency of the error which is attributed to the reasons above.

	1 Amp	2 Amp	3 Amp
As Built ANS	34.7	72.6	136.0
As Built EXP	34.4	68.1	133.8
Gap Pad ANS	N/A	N/A	105.0
Gap Pad EXP	31.4	53.3	100.2
AI Contacts ANS	30.7	56.6	99.8
AI Contacts EXP	31.3	51.7	90.2
Gap Pad and Contacts ANS	30.2	55.2	96.8
Gap Pad and Contacts EXP	30.3	48.2	89.1

Table 12: Comparing ANSYS and Experimental Results for Each Prototype

This study also exemplified how the optimization tool can be applied to solve engineering problems in the most effective manner. As mentioned previously, physical experimentation is quite expensive and time consuming, so finding areas where maximum heat flux occurs using the FEA tool and then improving the system at those points was shown to be an effective way to improve the motor.

The goal of this section was to show a way in which a finite element tool can be used as an aid in the redesign process. This was successfully done, making cheap and effective modifications to a motor, and testing and validating the results. In the big picture, this sort of analysis, optimization, and redesign cycle could be run on any system to improve its performance.

Overall, this group of studies was a success by showing yet another capability of FEA tools which can be applied in real world situations to help make design and modification decisions.

## CHAPTER IV

### **Conclusions and Future Works**

In order to explore the finite element tool, what it is, and how it is used, a history of the finite element method was presented. This method was first used in the early 1940s as a tool in the aircraft structural industry, and has grown into a tool used widely across a variety of engineering disciplines. It is clear that the finite element method is a very powerful tool that is capable of solving unique and complicated engineering problems. Much of the benefit of the tool comes in conjunction with the development of computer technology. The finite element method takes much computer power to solve complicated simultaneous equations, as well as powerful computer graphics to improve its results visualization and redesign capabilities. Finite element analysis software is increasingly being used in the design cycle, rather than as a solely analytical tool. Finite element analysis tools appear to be on a path towards having little to no user interaction and still providing reliable results. However, one of the most important things to note about FEA is that it is a tool to aid in engineering processes. Misuse of the tool is possible if care is not taken in understanding the fundamentals of the model and validating the results.

In Chapter 2, several finite element studies were performed and considered within the framework of the Adaptive Vehicle Make (AVM) program. Studies were run on two components of a small scale remote control vehicle. These studies were viewed through the lens of reliability, validation, and the applicable takeaways that can be gained from a finite element study. From the results, it is obvious that care must be taken in the

assumptions made for a study, as well as in the conclusions that can be drawn from the results. A fundamental understanding of the fundamental finite element method helps the user better utilize the finite element tool.

Next, a brushless flat motor was studied. The purpose of this section was to provide a thorough example of a system redesign aided by finite element analysis tools. The first step was to create a model of the system using CAD and FEA tools. The model was then validated with physical experimentation. Modifications were explored using the validated finite element model. Finally, to complete the redesign cycle and test the modifications, prototypes were created and then experimentally tested to confirm the expected results. This cycle of model, validate, redesign, prototype and test is a valuable tool in the design cycle, and is becoming faster, cheaper, and more reliable as finite element tools become more powerful. The cycle was successfully implemented, with error from FEA model to experimentation consistent and under 10 percent. Motor thermal performance was improved by 40 percent, allowing for increased operation capabilities of the motor.

Some future works that could build off of those presented here could include a study of a more complicated system, with several components that interact together. It would be interesting to study how modifications made by an optimization tool similar to the one presented here affect components in the framework of a larger system. As discussed, modeling the interaction of components in a system is one of the biggest challenges of modern day finite element analysis.

In conclusion, the biggest contributions of this thesis, supported by either the research presented or the FEA studies and experiments performed are as follows:

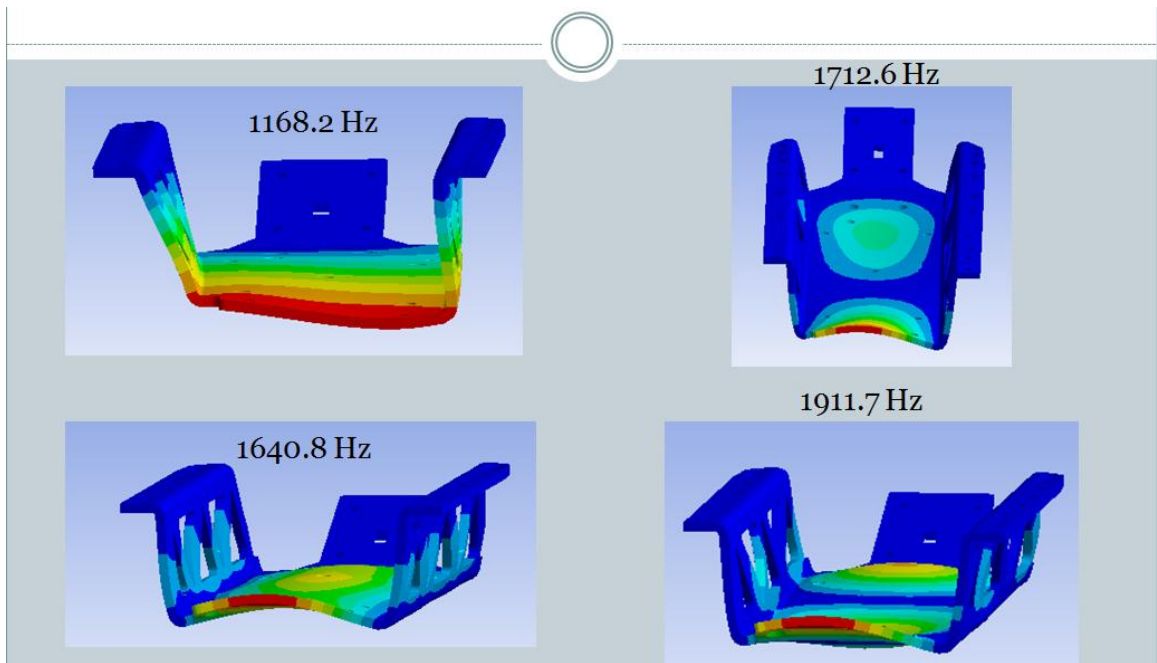
## **Contributions**

- Demonstrated an analysis of the Adaptive Vehicle Make project components using various finite element analysis studies.
- Created a thermal model of a brushless DC motor using computer aided design and finite element analysis tools.
- Validated the finite element motor model using physical experimentation.
- Designed heat sinking optimizations for a brushless DC motor using the finite element model.
- Created prototypes of the optimized motor to test the finite element analysis thermal results.
- Demonstrated a 40 percent increase in the thermal performance of a brushless DC motor.
- Demonstrated the redesign cycle on a brushless DC motor, showing how finite element analysis can aid in the process.

## APPENDIX A

### Chassis Modal Shapes

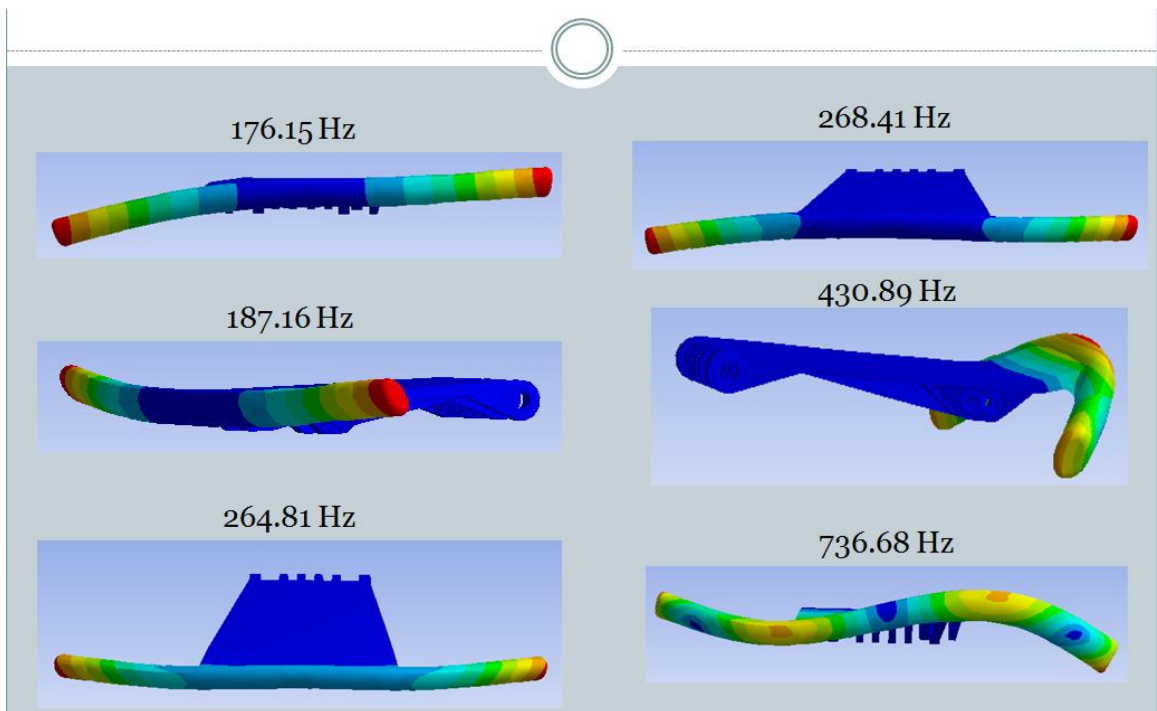
Natural frequency modal shape showing deformation of the main chassis at the first (top left), second (bottom left), third (top right), and fourth (bottom right) resonant frequencies.



## APPENDIX B

### Bumper Modal Shapes

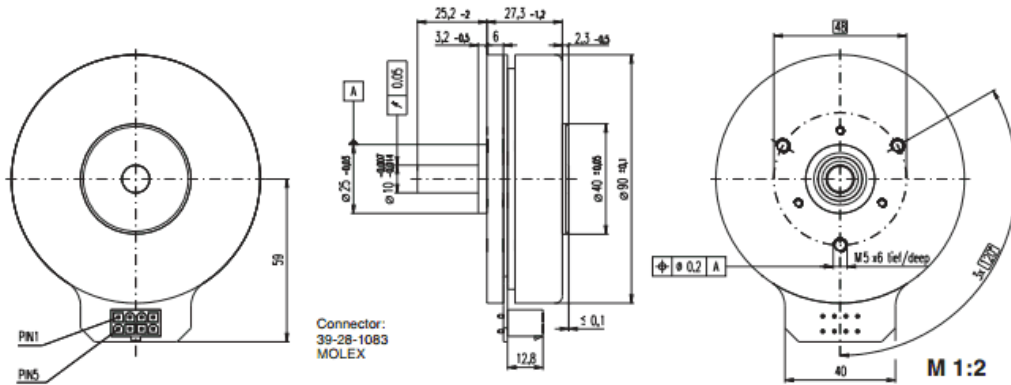
Natural frequency modal shape showing deformation of the front bumper at the first (top left), second (middle left), third (bottom left), fourth (top right), fifth (middle right), and sixth (bottom right) resonant frequencies.



# APPENDIX C

## Maxon EC Flat Motor Data Sheet

### EC 90 flat $\varnothing 90$ mm, brushless, 90 Watt



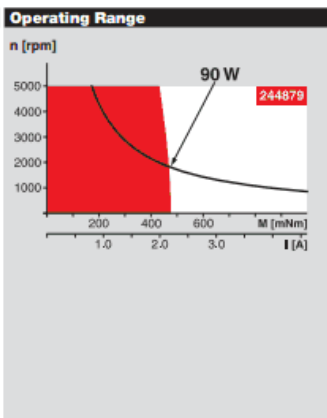
maxon flat motor

- Stock program
- Standard program
- Special program (on request)

Order Number	
with Hall sensors	323772      244879

Motor Data (provisional)		with Hall sensors	
Values at nominal voltage			
1	Nominal voltage	V	24.0      48.0
2	No load speed	rpm	3190      2080
3	No load current	mA	539      130
4	Nominal speed	rpm	2650      1640
5	Nominal torque (max. continuous torque)	mNm	387      494
6	Nominal current (max. continuous current)	A	5.39      2.12
7	Stall torque	mNm	4670      4530
8	Starting current	A	66.2      20.9
9	Max. efficiency	%	83      85
Characteristics			
10	Terminal resistance phase to phase	$\Omega$	0.363      2.30
11	Terminal inductance phase to phase	mH	0.264      2.50
12	Torque constant	mNm / A	70.5      217
13	Speed constant	rpm / V	135      44.0
14	Speed / torque gradient	rpm / mNm	0.697      0.466
15	Mechanical time constant	ms	22.3      14.9
16	Rotor inertia	gcm <sup>2</sup>	3060      3060

Specifications		
Thermal data		
17	Thermal resistance housing-ambient	1.89 K / W
18	Thermal resistance winding-housing	2.99 K / W
19	Thermal time constant windings	52.6 s
20	Thermal time constant motor	281 s
21	Ambient temperature	-40 ... +100°C
22	Max. permissible winding temperature	+125°C
Mechanical data (preloaded ball bearings)		
23	Max. permissible speed	5000 rpm
24	Axial play at axial load < 15 N	0 mm
	> 15 N	0.14 mm
25	Radial play	preloaded
26	Max. axial load (dynamic)	12 N
27	Max. force for press fits (static)	150 N
	(static, shaft supported)	8000 N
28	Max. radial loading, 7.5 mm from flange	30 N
Other specifications		
29	Number of pole pairs	12
30	Number of phases	3
31	Weight of motor	648 g



**Comments**

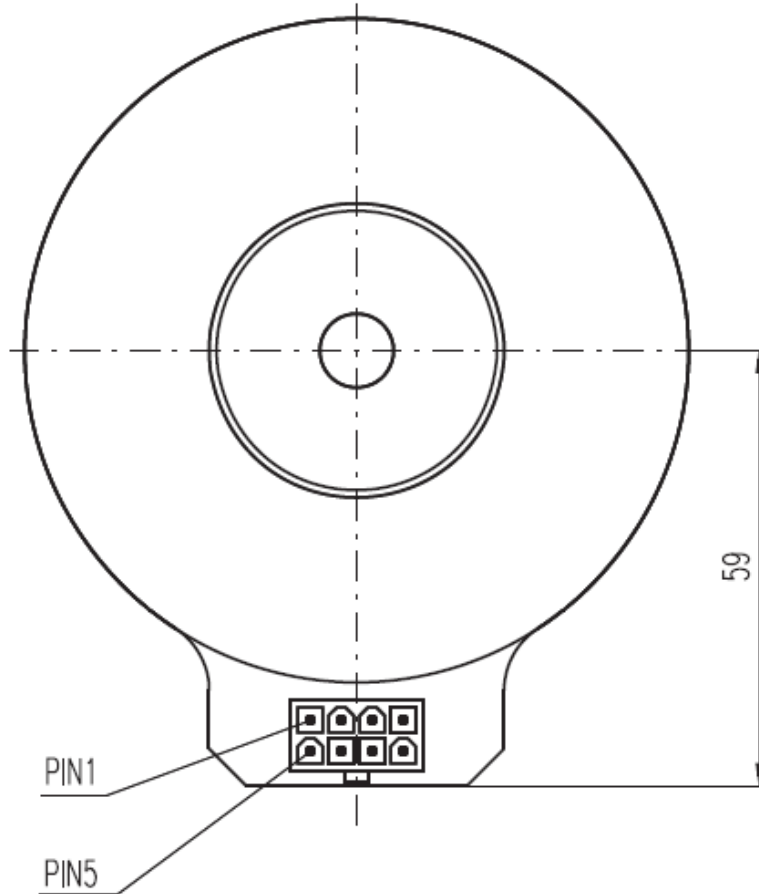
- Continuous operation**  
In observation of above listed thermal resistance (lines 17 and 18) the maximum permissible winding temperature will be reached during continuous operation at 25°C ambient.  
= Thermal limit.
- Short term operation**  
The motor may be briefly overloaded (recurring).
- Assigned power rating**

Values listed in the table are nominal.



## APPENDIX D

### Maxon EC Flat Motor Pin Schematic



#### Connection

Pin 1	Hall sensor 1
Pin 2	Hall sensor 2
Pin 3	4.5 ... 24 VDC
Pin 4	Motor winding 3
Pin 5	Hall sensor 3
Pin 6	GND
Pin 7	Motor winding 1
Pin 8	Motor winding 2

# APPENDIX E

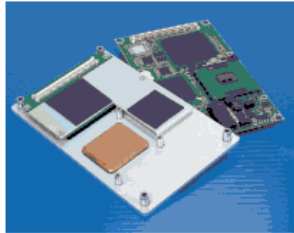
## Gap Pad 1500 Data Sheet

### Gap Pad® 1500

Thermally Conductive, Un-Reinforced Gap Filling Material

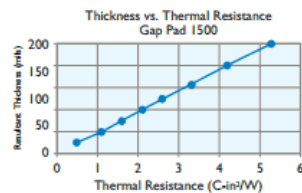
#### Features and Benefits

- Thermal conductivity: 1.5 W/m-K
- Un-reinforced construction for additional compliancy
- Conformable, low hardness
- Electrically isolating



Gap Pad 1500 has an ideal filler blend that gives it a low-modulus characteristic that maintains optimal thermal performance yet still allows for easy handling. The natural tack on both sides of the material allows for good compliance to adjacent surfaces of components, minimizing interfacial resistance.

Note: Resultant thickness is defined as the final gap thickness of the application.



TYPICAL PROPERTIES OF GAP PAD 1500			
PROPERTY	IMPERIAL VALUE	METRIC VALUE	TEST METHOD
Color	Black	Black	Visual
Reinforcement Carrier	—	—	—
Thickness (inch) / (mm)	0.020 to 0.200	0.508 to 5.080	ASTM D374
Inherent Surface Tack (1 sided)	2	2	—
Density (Bulk Rubber) (g/cc)	2.1	2.1	ASTM D792
Heat Capacity (J/g-K)	1.0	1.0	ASTM E1269
Hardness (Bulk Rubber) (Shore 00) (1)	40	40	ASTM D2240
Young's Modulus (psi) / (kPa) (2)	45	310	ASTM D575
Continuous Use Temp (°F) / (°C)	-76 to 392	-60 to 200	—
<b>ELECTRICAL</b>			
Dielectric Breakdown Voltage (Vac)	>6000	>6000	ASTM D149
Dielectric Constant (1000 Hz)	5.5	5.5	ASTM D150
Volume Resistivity (Ohm-meter)	10 <sup>11</sup>	10 <sup>11</sup>	ASTM D257
Flame Rating	V-0	V-0	UL 94
<b>THERMAL</b>			
Thermal Conductivity (W/m-K)	1.5	1.5	ASTM D5470
<b>THERMAL PERFORMANCE vs. STRAIN</b>			
	Deflection (% strain)		
	10	20	30
Thermal Impedance (°C-in <sup>2</sup> /W) 0.040" (3)	1.62	1.50	1.33

1) Thirty second delay value Shore 00 hardness scale. 2) Young's Modulus, calculated using 0.01 in/min. step rate of strain with a sample size of 0.79 inch. 3) The ASTM D5470 test fixture was used. The recorded value includes interfacial thermal resistance. These values are provided for reference only. Actual application performance is directly related to the surface roughness, flatness and pressure applied.

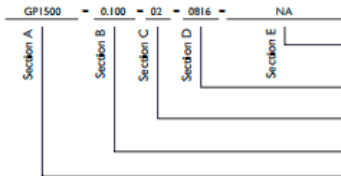
#### Typical Applications Include:

- Telecommunications
- Computer and peripherals
- Power conversion
- RDRAM™ memory modules / chip scale packages
- Areas where heat needs to be transferred to a frame chassis or other type of heat spreader

#### Configurations Available:

- Sheet form and die-cut parts

#### Building a Part Number



#### Standard Options

44 example  
 NA = Selected standard option. If not selecting a standard option, insert company name, drawing number, and revision level.  
 0816 = Standard sheet size 8" x 16", or 00 = custom configuration  
 02 = Natural tack, both sides  
 Standard thicknesses available: 0.020", 0.040", 0.060", 0.080", 0.100", 0.125", 0.160", 0.200"  
 GP1500 = Gap Pad 1500 Material

Note: To build a part number, visit our website at [www.bergquistcompany.com](http://www.bergquistcompany.com).

## References

- [1] Adaptive Vehicle Make, DARPA,  
[http://www.darpa.mil/Our\\_Work/TTO/Programs/Adaptive\\_Vehicle\\_Make\\_\\_\\_%28AVM%29.aspx](http://www.darpa.mil/Our_Work/TTO/Programs/Adaptive_Vehicle_Make___%28AVM%29.aspx)
- [2] ANSYS, Swanson, J. A., ANSYS-Engineering Analysis Systems User's Manual, Swanson Analysis Systems, Inc., Johnson Rd., P.O. Box 65, Houston, PA, 15342.
- [3] Archer, J. S., "Consistent Matrix Formulations for Structural Analysis Using Finite-Element Techniques," Journal of the American Institute of Aeronautics and Astronautics, Vol. 3, No. 10, pp. 1910-1918, 1965.
- [4] Argyris, J. H., and Kelsey, S., Energy Theorems and Structural Analysis, Butterworths, London, 1960 [collection of papers published in Aircraft Engineering in 1954 and 1955].
- [5] Argyris, J. H., "Recent Advances in Matrix Methods of Structural Analysis", Progress in Aeronautical Science, Vol. 4, Pergamon Press, New York, 1964.
- [6] Arpaci, Vedat S., and Vedat S. Arpaci. Conduction heat transfer. Reading: Addison-Wesley, 1966.
- [7] Baja 5sc, Super Sport, HPI Racing, # 105735  
<http://www.hpiracing.com/en/kit/105735>
- [8] Bergquist Company, The, 18930 W. 78th Street, Chanhassen, MN, 55317,  
<http://www.bergquistcompany.com>

- [9] Clough, R. W., “The Finite Element Method in Plane Stress Analysis”, Proceedings, American Society of Civil Engineers, 2nd Conference on Electronic Computation, Pittsburgh, PA, pp. 345-378, Sept. 1960.
- [10] Clough, R. W., and Rashid, Y., “Finite Element Analysis of Axisymmetric Solids”, Journal of the Engineering Mechanics Division, Proceedings of the American Society of Civil Engineers, Vol. 91, pp. 71-85, Feb. 1965.
- [11] “Computer Misuse – Are We Dealing with a Time Bomb? Who is to Blame and What Are We Doing about It? A Panel Discussion”, in Forensic Engineering, Proceedings of the First Congress, K. L. Rens (ed.), American Society of Civil Engineers, Reston, VA, 1997, pp. 285-336.
- [12] Conover, Dave. “Verification and Validation of FEA Simulations”. Integration of Simulation Technology into the Engineering Curriculum. Cornell University. 2008.
- [13] Cook, Robert D., Malkus, David S., Concepts and Applications of Finite Element Analysis. John Wiley & Sons, 2007.
- [14] Courant, R., “Variational Methods for the Solution of Problems of Equilibrium and Variations”, Bulletin of the American Mathematical Society, Vol. 49, pp. 1-23, 1943.
- [15] Coz Díaz, J. J., P.J. García Nieto, C. Betegón Biempica, M.B. Prendes Gero, “Analysis and optimization of the heat-insulating light concrete hollow brick walls design by the finite element method,” Applied Thermal Engineering, Volume 27, Issues 8–9, June 2007, Pages 1445-1456.

- [16] Gallagher, R. H., Padlog, J., Bijlaard, P. P., "Stress Analysis of Heated Complex Shapes", Journal of the American Rocket Society, Vol. 32, pp. 700-707, 1962.
- [17] Gallagher, R. H., and Padlog, J., "Discrete Element Approach to Structural Stability Analysis", Journal of the American Institute of Aeronautics and Astronautics, Vol. 1, No. 6, pp 1437-1439, 1963.
- [18] Grafton, P. E., Strome, D. R., "Analysis of Axisymmetric Shells by the Direct Stiffness Method," Journal of the American Institute of Aeronautics and Astronautics, Vol. 1, No. 10, pp. 2342-2347, 1963.
- [19] Hrennikoff, A., "Solution of Problems in Elasticity by the Frame Work Method," Journal of Applied Mathematics, Vol. 8, No. 4, pp. 169-175, Dec. 1941.
- [20] Hughes, Thomas JR. The finite element method: linear static and dynamic finite element analysis. DoverPublications.com, 2012.
- [21] Incropera, Frank, and David DeWitt. "Introduction to heat transfer." (1985).
- [22] Johnson, Walter, et al. "META II: Formal Co-Verification of Correctness of Large-Scale Cyber-Physical Systems During Design" (Mod 0006). Volume 2. PALO ALTO RESEARCH CENTER INC (PARC) PALO ALTO CA, 2012.
- [23] Kays, William Morrow, Michael E. Crawford, and Bernhard Weigand. Convective heat and mass transfer. Vol. 3. New York: McGraw-Hill, 1993.
- [24] Kurtoglu, Tolga, et al. "A Functional Failure Reasoning Methodology for Evaluation of Conceptual System Architectures". Volume 21, Issue 4. Research in Engineering Design. 2010.

- [25] Levy, S., “Computation of Influence Coefficients for Aircraft Structures with Discontinuities and Sweepback”, *Journal of Aeronautical Sciences*, Vol. 14, No. 10, pp. 547-560, Oct. 1947.
- [26] Levy, S., “Structural Analysis and Influence Coefficients for Delta Wings”, *Journal of Aeronautical Sciences*, Vol. 20, No. 7, pp. 449-454, July 1953.
- [27] Logan, Daryl L., *A First Course in the Finite Element Method*, Cengage Learning, 2012.
- [28] Martin, H. C., “Plane Elasticity Problems and the Direct Stiffness Method”, *The Trend in Engineering*, Vol. 13, pp. 5-19, Jan. 1961.
- [29] Martin, H. C., “Finite Element Analysis of Fluid Flows,” *Proceedings of the Second Conference on Matrix Methods in Structural Mechanics*, Wright-Patterson Air Force Base, Ohio, pp. 517-535, Oct. 1968.
- [30] McHenry, D., “A Lattice Analogy for the Solution of Plane Stress Problems,” *Journal of Institution of Civil Engineers*, Vol. 21, pp. 59-82, Dec. 1943
- [31] Melosh, R. J., “A Stiffness Matrix for the Analysis of Thin Plates in Bending”, *Journal of the Aerospace Sciences*, Vol. 28, No. 1, pp. 34-42, Jan. 1961.
- [32] Melosh, R. J., “Structural Analysis of Solids”, *Journal of the Structural Division, Proceedings of the American Society of Civil Engineers*, pp. 205-223, Aug. 1963.
- [33] Nagler, Oliver, Michael Trost, Bernd Hillerich, Frank Kozlowski, “Efficient design and optimization of MEMS by integrating commercial simulation tools,” *Sensors and Actuators A: Physical*, Volume 66, Issues 1–3, 1 April 1998, Pages 15-20.

- [34] Rai, Rahul, et al. "Simulation-Based Design of Aircraft Electrical Power Systems." Proceedings of the 8th Modelica Conference. 2011.
- [35] Reddy, J. N., "The Finite Element method: A Child of the Computer Age," Sooner Shamrock, 23-36, Fall 1978.
- [36] Reddy, J. R., An Introduction to the Finite Element Method, McGraw-Hill, 2006.
- [37] Riedel, W., "Beiträge zur Lösung des ebenen Problems eines elastischen Körpers mittels der Airyschen Spannungsfunktion", Zeitschrift für Angewandte Mathematik und Mechanik, Vol. 7, No. 3, 1927, pp. 169-188 (discussion by C. Weber, Vol. 8, No. 2, 1928, pp. 159-160).
- [38] Robinson, J., Early FEM Pioneers, Robinson and Associates, Dorset, UK, 1985
- [39] Singleton Jr, John Matthew, Mullen, Benjamin. "ANSYS 12 – Plate With a Hole Optimization," SimCafe 2011.
- [40] Smith, G. E., "The Dangers of CAD", Mechanical Engineering, Vol. 108, No. 2, 1986, pp. 58-64.
- [41] Staton, D.; Boglietti, A.; Cavagnino, A., "Solving the More Difficult Aspects of Electric Motor Thermal Analysis in Small and Medium Size Industrial Induction Motors," Energy Conversion, IEEE Transactions on , vol.20, no.3, pp.620,628, Sept. 2005
- [42] Staton, D.A.; Cavagnino, A., "Convection Heat Transfer and Flow Calculations Suitable for Electric Machines Thermal Models," Industrial Electronics, IEEE Transactions on , vol.55, no.10, pp.3509,3516, Oct. 2008

- [43] Symonds, P. S., and Yu, T. X., "Counterintuitive Behavior in a Problem of Elastic-Plastic Beam Dynamics", ASME Journal of Applied Mechanics, Vol. 52, No. 3, 1985, pp. 517-522.
- [44] Szabo, B. A., and Lee, G. C., "Derivation of Stiffness Matrices for Problems in Plane Elasticity by Galerkin's Method," International Journal of Numerical Methods in Engineering, Vol. 1, pp. 301-310, 1969.
- [45] Tribus, Myron. "Rational Descriptions, Decisions, and Design". Pergamon Press. 1969.
- [46] Turner, M. J., Clough, R. W., Martin, H. C., Topp, L. J., "Stiffness and Deflection Analysis of Complex Structures", Journal of the Aeronautical Sciences, Vol. 23, No. 9, 1956, pp. 805-823.
- [47] Turner, M. J., "Large Deflections of Structures Subject to Heating and External Loads", Journal of Aeronautical Sciences, Vol. 27, No. 2, pp. 97-107, Feb. 1960.
- [48] Weighardt, K., "Über einen Grenzübergang der Elastizitätslehre und Seine Anwendung auf die Statik hochgradig statisch unbestimmter Fachwerke," Verhandlungen des Vereins zur Beförderung des Gewerbfleißes, Vol. 85, 1906, pp. 139-176
- [49] Wiedenman, Nathan, LTC, The Next Generation: How DARPA Democratizes Design, Maker Faire Bay Area 2012, San Mateo, CA, May 19, 2012
- [50] Williamson, F., "A Historical Note on the Finite Element Method," International Journal for Numerical Methods in Engineering, Vol. 15, No. 6, 1980, pp. 930-934



- [51] Wilson, E. L., "Structural Analysis of Axisymmetric Solids", Journal of the American Institute of Aeronautics and Astronautics, Vol. 3, No. 12, pp. 2269-2274, Dec. 1965.
- [52] Wilson, E. L., and Nickel, R. E., "Application of the Finite Element Method to Heat Conduction Analysis," Nuclear Engineering and Design, Vol. 4, pp. 276-286, 1966.
- [53] Yong-hai, Wu, Wang Feng, and Ma Cong-bing. "Optimization design of a light truck frame based on ANSYS." Computer Science & Education (ICCSE), 2012 7th International Conference on. IEEE, 2012.
- [54] Zienkiewicz, O. C., and Cheung, Y. K., "Finite Elements in the Solution of Field Problems," The Engineer, pp. 507-510, Sept. 24, 1965.
- [55] Zienkiewicz, O. C., Watson, M., and King, I. P., "A Numerical method of Visco-Elastic Stress Analysis," International Journal of Mechanical Sciences, Vol. 10, pp. 807-827, 1968.
- [56] Zienkiewicz, O. C., and Parekh, C. J., "Transient Field Problems: Two-Dimensional and Three-Dimensional Analysis by Isoparametric Finite Elements," International Journal of Numerical Methods in Engineering, Vol. 2, No. 1, pp. 61-71, 1970.